SKB

TECHNICAL REPORT 88-26

Geological evidence of smectite longevity
The Sardinian and Gotland cases

Roland Pusch, Ola Karnland

Clay Technology AB

December 1988

SVENSK KÄRNBRÄNSLEHANTERING AB
SWEDISH NUCLEAR FUEL AND WASTE MANAGEMENT CO

BOX 5864 S-102 48 STOCKHOLM
TEL 08-665 28 00 TELEX 13108-SKB

GEOLOGICAL EVIDENCE OF SMECTITE LONGEVITY

The Sardinian and Gotland Cases

Roland Pusch, Ola Karnland

Clay Technology AB

December 1988

Geological Evidence of Smectite Longevity

The Sardinian and Gotland Cases

Roland Pusch
Ola Karnland

Clay Technology AB

December 1988

CONTENTS

GEOLOGICAL EVIDENCE OF SMECTITE LONGEVITY -
The Sardinian and Gotland cases

SUMMARY

Parallel to the systematic experimental and theoretical attempts that are being made for identification of the criteria which determine the chemical stability of smectite minerals of clay buffer materials in repositories for high level radioactive repositories, search is going on for geological evidence of natural smectite clay materials that have been exposed to conditions that are similar to those in repositories. Cases in which heating to 90°C or more for long periods has taken place, are of particular interest, the only example that has been considered so far, although not yet in great detail, being the Ordovician Kinnekulle bentonite sequence. The present report describes two other bentonite layers, one of Miocenic age located at central Sardinia (Busachi), and the other of Ordovician age, forming a basal stratum of southern Gotland, (Hamra), Sweden. They both serve as excellent examples of the survival potential of montmorillonite-rich clays.

The more than 10 m thick Sardinian bentonite bed, which is located below 2 m of rhyolite rock and presently exploited for the production of commercial bentonite, was very significantly heated when the magma moved in and covered it. The upper meter was heated to more than 200°C for several days, while at more than 4 m depth, the temperature did not exceed 80°C. The tests show that the smectite content was not reduced to less than 60 % in any part of the layer sequence, while slight cementation was caused by precipitation of heat-released silica in the uppermost layer.

The 0.3 m thick bed on Gotland is presently located at 515 m depth. Various investigations indicate that it has been exposed to an effective pressure of 30 MPa and a temperature of 110°C for several million years due to burial under almost 3 km of Devonian sediments. The content of smectite is around 25 % of the bulk material, and 30-40 % of the clay fraction. Illite appears to have been neoformed in small voids of the smectite matrix and the identified apparent I/S material is suggested to

consist of mixed-layer minerals with hydrous mica and Ca or Na locked in instead of K, which would be the conventional interpretation. The earlier developed alteration model appears to be valid and it is extended in the present report on the basis of the findings.

1 INTRODUCTION

Various techniques have been tested for the characterization of smectitic clays in the systematic SKB-related research work and the present study made use of the most pertinent ones, among which XRD methods for quantitative clay mineral determination, electron microscopy, permeability tests and creep studies yield most information. By this, the content and distribution of smectite minerals in the clays have been identified with an accuracy that allows for interpretation of the alteration processes that have taken place. Particularly valuable results have been obtained by application of a refined Fourier technique for evaluating the nature and ordering of mixed-layer mineral sequences in the Ordovician of clay from Gotland and thereby its mineralogical history, and by conducting analytical electron microscopy for the same purpose. Further efforts to identify the geological scenarios that led to the present physical and mineralogical states of this clay were made by involving Dr Sven Snäll, Swedish Geological Survey, for evaluating paleotemperatures from I/S considerations and from the crystallization index of illite, as well as by asking for OPAB's conclusions from their oil prospect activities in the Hamra area.

2 CLAY MATERIALS

2.1 Sardinian bentonite

2.1.1 Geological history

The bentonite at Busachi, central Sardinia (cf.Fig.1), was formed in the Miocene when the larger part of Sardinia became submerged in the sea.

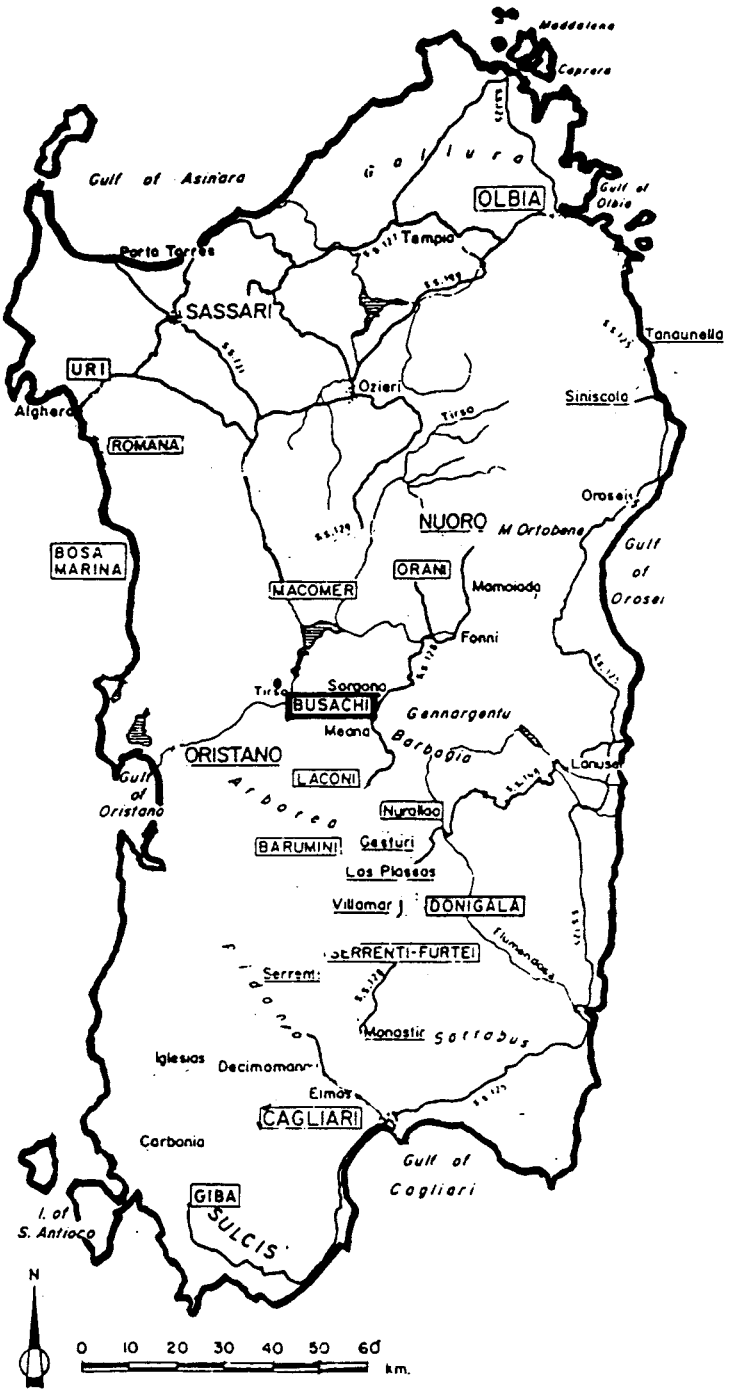

Fig.1. Location of the Busachi site

The eruptive cycle that started in the Oligocene and continued in the Miocene, gave birth to the bentonite according to the following probable genetic model (Mezzetti & Gorelli):

1. Miocenic submarine eruption of fine mesosilic pyroclastics

2. Fast argillification due to contact of the hot glassy particles with sea water

3. Transport and sorting of the altered material

4. Deposition of the smectite-rich fraction in calm water

Magma outflow over Sardinian bentonite clay beds has occurred on certain sites, and this is thought to be the case for the Busachi area (Sud--Chemie Italia). The obvious undulation of the contact between the rock and the more than 10 m thick clay sediment series suggests that the clay was in a rather soft state at the eruption, which may have taken place in shallow water. Since the actual conditions are not known and they certainly determined the temperature evolution in the clay series, which is of course of fundamental importance in the present context, different possible scenarios have been assumed in the mathematical back-calculation of the heating event.

Two entirely different conditions were considered for evaluation of the temperature history, one assuming that the magma moved in over the clay that formed sea bottom at 10 m depth, the other being based on the assumption that the magma moved in on dry land formed by the clay series. In the first case it is assumed that the rhyolite formed a 2 m thick top bed, i.e. its present thickness, and that the clay had a consistency corresponding to its liquid limit (about 100 %) throughout the heating period. Water of a temperature of 30°C or 75°C is assumed to have covered the area for at least 6 months after the eruption. In the second, dry case, it is assumed that the rhyolite formed a 2 m thick top bed over somewhat more consolidated clay with a water content of 30 % .

The present stratigraphy is generalized in Fig.2. It is assumed that the clay has not been exposed to a significantly higher vertical effective pressure than at present, which is in the range of 50 to 200 kPa.

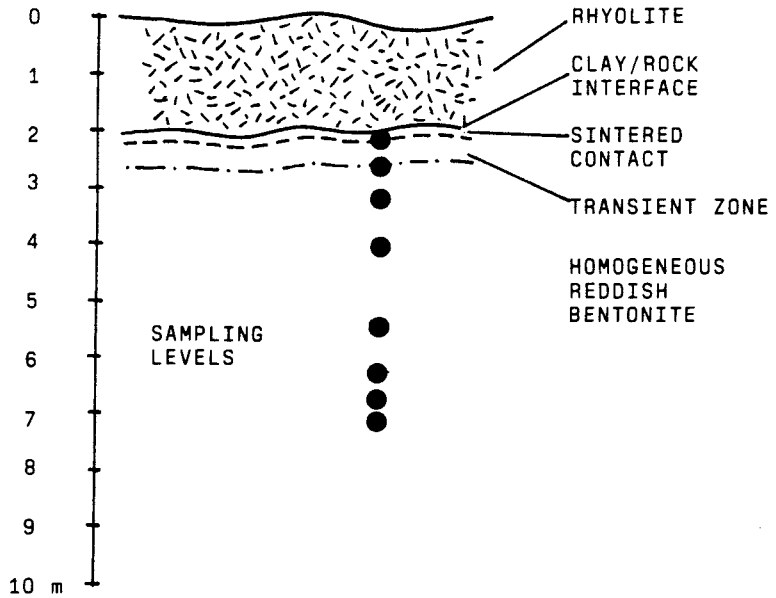

Fig.2. Stratigraphy of the sampling site at Busachi

2.1.2 Temperature history

The heat evolution in the three cases, i.e. the submerged clay sediment with different water temperatures, and the dry-crust version, was calculated by applying FEM, using heat conductivity values in the range of 0.7 - 0.9 W/m,K for the clay and 2.3 W/m,K for the rock, and a heat capacitivity of 1600 - 2500 Ws/kg,K and 800 Ws/kg,K for the clay and rock, respectively. For the dry crust case it was assumed that the heat removal by air flow was characterized by the heat transfer coefficient value 10 W/m^2,K, while the boundary condition for the submerged systems was given by an assumed constant water temperature of 30, and 75^{o}C, respectively. In the latter cases, rather rapid water convection in the 10 m deep estuary was assumed to have yielded constant temperature for at least half a year.

We see from Fig.3 that for the dry crust case the temperature at 2.2 m depth, i.e. 0.2 m below the rock/clay interface was 800°C for 1 day only and that it dropped to 500°C after one week and to 200°C after 2 months. The clay samples from this level were brighter and stiffer than those from larger depth but they could still be rather easily disintegrated in water. Closer to the rock the clay was much harder and gave the impression of being sintered. Fig.4 shows the temperature decay at 0.5 m depth from the rock interface and from this diagram we conclude that the heating period was very short.

The wet cases do not yield very different heat evolution patterns as shown by Table 1. For the particular purpose of correlating the alteration of physical and chemical properties with temperature, it is conservative to apply the lowest evaluated temperatures, and the wet case with a water temperature of 75°C is therefore referred to although the two other scenarios may be more feasible. It is concluded also, that the assumption of a sedimentary origin of the clay series is not critical to the derivation of the heating history. The clay may well have resulted from in situ hydrothermal rock alteration.

Table 1. Calculated maximum temperature of the Busachi bentonite (°C)*

Depth below rock boundary, m	Dry crust case	Wet case, 30°C	Wet case, 75°C
0.2	800	750	700
0.7	300	280	250
1.2	170	155	150
2.1	80	65	60
3.5	50	35	25
4.3	35	25	20
4.7	25	20	20
5.1	20	20	20

* 20°C is taken as the minimum temperature

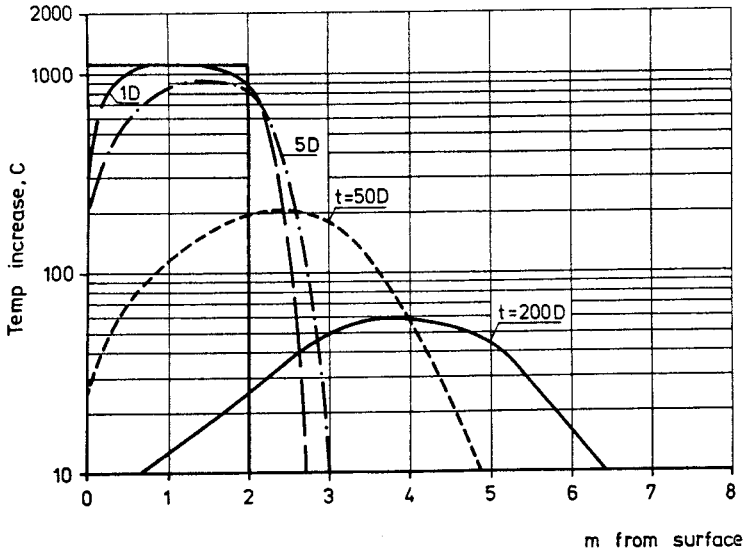

Fig.3. Temperature profile development at different depths from the upper boundary of the 2 m thick rock slab for the dry crust case (Busachi)

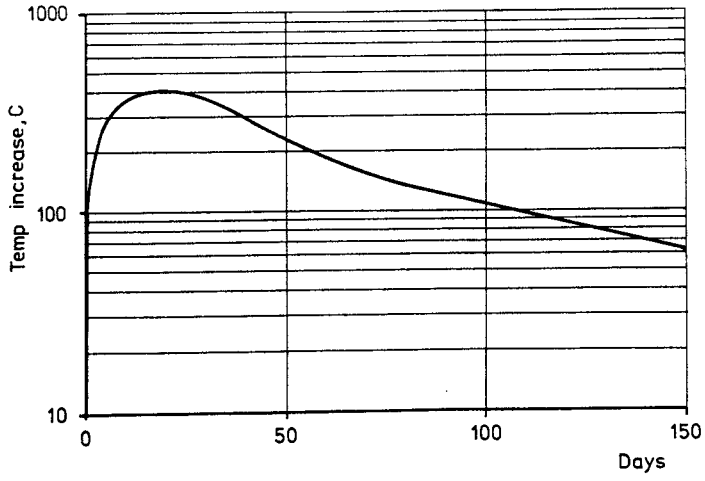

Fig.4. Temperature evolution at 0.5 m depth below the rock contact in the dry crust case (Busachi)

2.1.2 General properties

Samples were kindly put to the authors'disposal by Dr De Angelis, Sud-Chemie Italia, for the laboratory study. They were slightly dried and could not be used for rheological testing, but fragments with a size of 0.1 to 1 cm^3 appeared to be undisturbed and could be investigated with respect to their microstructural constitution.

2.1.2.1 *Grain size distribution*

The material was found to contain rather coarse grains, particularly in the uppermost layer, but the clay content was still high. The coarser grains caused substantial trouble in the preparation of ultrathin sections for the electron microscopy.

The preparation for the grain size determination included removal of millimeter-sized grains, drying at 105^{o}C, and dispersion in distilled water with sodium pyrophosphate by use of ultrasonic treatment for a few hours. Hydrometer analyses were made and they showed that the clay content of the layer located at 0.5 m depth was about 75 %, while it was 80 - 90 % down to 4 m depth and about 65 % at 5 m depth.

2.1.2.2 *Soil physical data*

With the exception of the 1 - 2 dm of clay forming the contact with the overlying rock, the reddish material is stiff but plastic. The water content of the samples ranged from 6 % at 0.2 m distance from the rock interface to about 30 % at 0.5 m distance and remained almost constant at this level down to the investigated depth. Some drying of the samples had most certainly taken place at the excavation and transportation.

The liquid limit was determined of samples from 0.5 m and 5 m distance from the rock/clay interface. The first-mentioned part of the clay series has w_L= 72 %, while for the lower part w_L= 92 %. This indicates that the clay, which is calcium-saturated, has a very high content of

smectite except for the sintered contact zone. This is in agreement with the fact that almost the entire clay series is used as raw material for the bentonite production of Sud-Chemie Italia, the montmorillonite content of the clay fraction typically ranging between 70 and 90 % by weight.

2.1.2.3 *Chemical data*

Typical chemical data of the iron-rich bentonite are given in Table 1. They are typical also of the commercially available clay materials offered by Sud-Chemie Italia.

Table 1. Chemical composition of the Busachi bentonite

Element	Concentration, %
SiO_2	55 - 60
Al_2O_3	16 - 20
Fe_2O_3	3 - 6
MgO	1 - 3
CaO	3 - 5
Na_2O	0.2

2.1.2.4 *Mineralogical data*

The bentonite clay series has been reported to be rich in dioctahedral montmorillonite, with Ca as major adsorbed cation, major accessory minerals in the clay fraction being cristobalite, opal, and zeolites. Carbonates are present to about 2 % in the natural clay, mostly in the coarser fractions, which also hold quartz and feldspar minerals. There are clasts of plagioclase with glass inclusions which certify that the clay is of volcanic origin.

The present study included determination of the cation exchange capacity and a Reynolds-type XRD analysis for quantitative determination of the smectite content.

The cation exchange capacity was determined by the Swedish Geological Survey, applying the following procedure: 8 g of clay material representing the clay fraction was dispersed in 100 ml of $SrCl_2$ solution and mechanically agitated for 24 hours. The clay was then washed seven times with distilled water, and subsequently with 70 % alcohol solution. After drying at 105°C the strontium content was determined and the cation exchange capacity evaluated. It was about 90 meq/100 g for samples taken 0.2 - 1.0 m from the clay/rock interface and 96 to 103 meq/100 g below that. This supports the conclusion from the determination of the consistency limit w_L that the montmorillonite content of the clay fraction is 70 - 90 % , except for the part closest to the rock where this content may be about 60 - 70 % .

The XRD determination was made by the Swedish Geological Survey with oriented minus 2 micron specimens and compacted specimens containing larger particles. The (001) peaks were found to be in the range of 13.6 to 15.2 Å before ethylene glycol treatment and 16.3 to 16.7 after glycolation. The individual data are shown in Table 2, from which it is concluded that the clay fraction consists of very pure Ca montmorillonite. Quartz and some 10 Å mineral are the only clearly discernible accessory components. Fig.5 shows the recorded XRD pattern.

Table 2. (001) reflections of the clay fraction extracted from the Busachi clay samples

Depth below clay/rock interface, m	Untreated Å	EG-treated Å
0.2	14.9	16.3
0.7	14.7	16.7
1.2	14.9	16.4
2.1	14.7	16.7
3.5	14.9	16.5
4.3	15.2	16.7
4.7	14.7	16.7
5.1	13.6	16.7

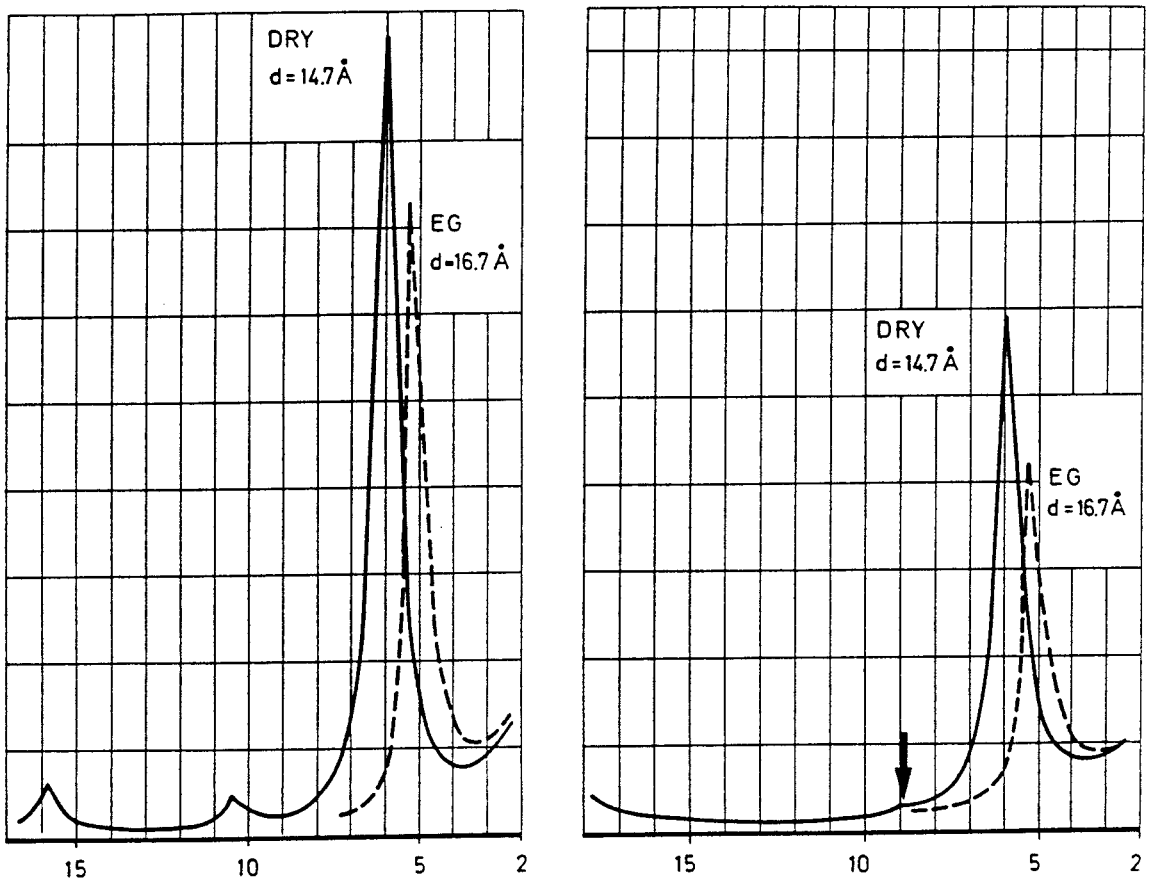

Fig.5. XRD diagrams of the clay fraction of material from 0.2 m (right) and 4.7 m (left) distance from the clay/rock interface. Bottom figures give 2θ. Arrow points at small 10 Å peak.

XRD diagrams were taken as a basis for quantitative analysis of two of the samples, i.e. one from 0.7 and one from 4.7 m depth below the clay/rock contact. The evaluation was made by Mikael Erlström, SGAB, Lund, who applied Reynolds' technique using pyrophyllite as reference clay mineral (1). The essential parameters are given in Table 3 together with the evaluated montmorillonite contents.

Table 3. Parameters obtained by applying Reynolds' method (Erlström)

Depth below clay/rock interface. m	Refl.	I	MIF	1/MIF	%	% Mo[a]	% I[b]
0.7	001 Py[c]	54	2.8	19	5		
	001 I	54	1.0	54			
	005 Mo	296	1.06	313	95	77	14
4.7	001 Py	58	3.1	19	5		
	001 I	38	1.0	38			
	005 Mo	350	1.06	330	95	88	10

a) Montmorillonite, b) 10 Å phyllosilicate mineral, c) Pyrophyllite

This study shows that the montmorillonite content of the investigated samples is in the range of 80 - 90 % , which is in very good agreement with the conclusions from the consistency and CEC determinations. One would expect the 10 Å minerals to be hydrous mica of the illite type but it may possibly be a matter of permanently collapse of montmorillonite or beidellite due to the heating. If so, sodium or calcium may be locked in interlamellar positions yielding a brammalite-type mineral.

Putting all the information on the composition and physical state of the Busachi clay material together one arrives at the montmorillonite content of the clay fraction that is given in Table 4.

2.1.3 Microstructural constitution

Samples were prepared for optical microscopy (30 microns thick sections) and for transmission electron microscopy (300 - 500 Å) for correlation of the microstructure, clay mineralogy, and bulk physical properties.

Table 4. Major water content, temperature, and montmorillonite content data of the Busachi clay series

Depth below clay/rock interface, m	Water content, %	Max. temperature, °C	Montmorillonite content of the clay frac., %
0.2	6	700	60 - 70
0.7	27	250	70 - 75
1.2	29	150	70 - 80
2.1	30	60	75 - 85
3.5	27	25	70 - 80
4.3	36	20	75 - 90
4.7	32	20	85 - 90
5.1	28	20	70 - 80

2.1.3.1 *Light microscopy*

Only the clay material from the "contact zone", i.e. 0.2 - 0.5 m depth, has been investigated by light microscopy. This study showed that the characteristic wavy microstructural pattern of interwoven montmorillonite stacks was retained despite the strong heat pulse of several hundred centigrades (Fig.6). Another preserved structural feature was the alignment of the stacks caused by the sedimentation and consolidation. Careful inspection of the micrographs revealed that recrystallization took place forming millimeter-sized grains with very sharp boundaries and corners, but there are also clear indications of strong weathering. Thus, one concludes that considerable solution and precipitation took place in the short hydrothermal treatment that the uppermost part of the clay series underwent.

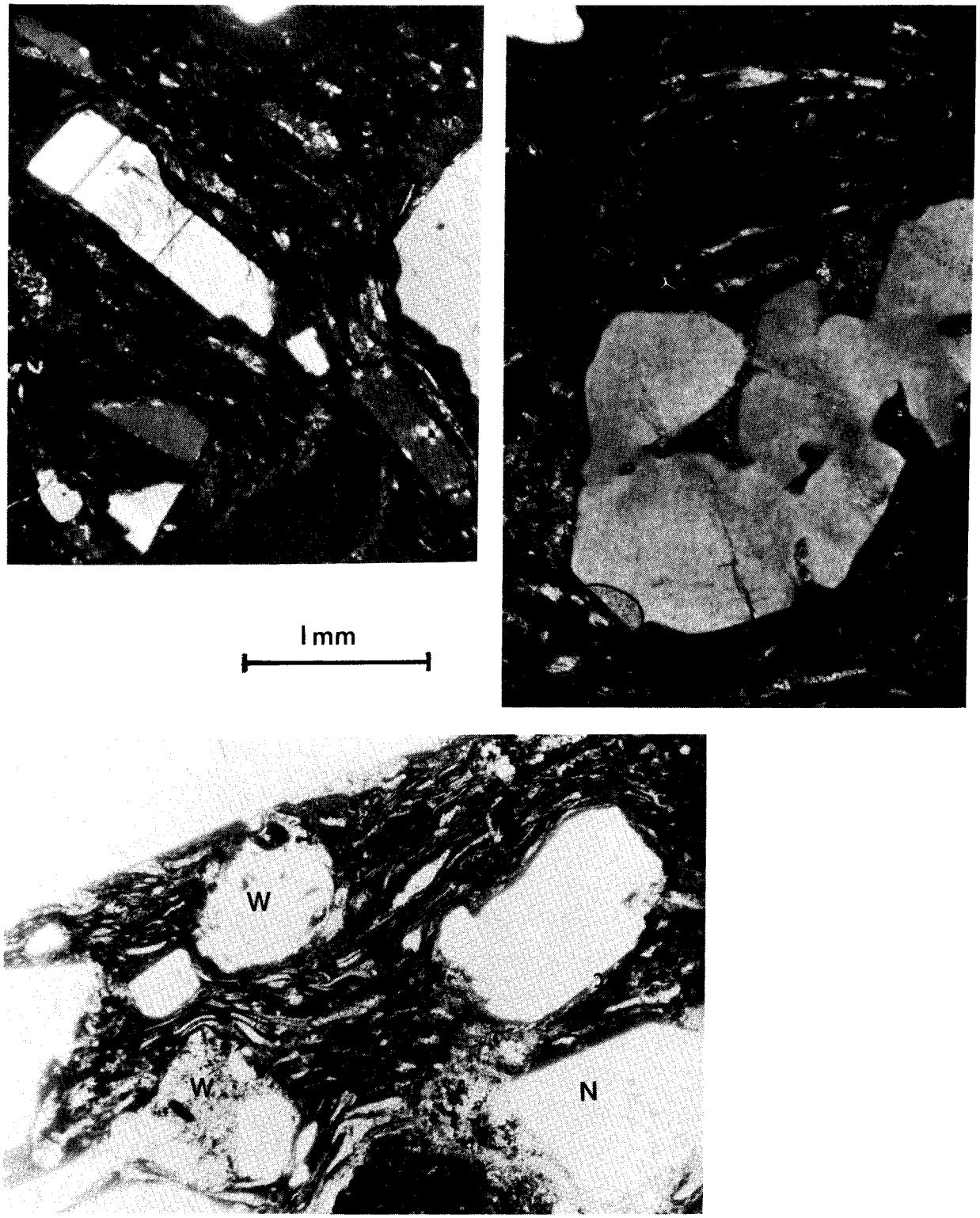

Fig.6. Typical features of the clay located a few decimeters from the clay/rock interface. Upper: Grains with very sharp contours, assumed to have been formed by recrystallization. Lower: Wavy matrix of smectite with weathered grains (W) and presumably neoformed crystals (N).

2.1.3.2 *Electron transmission microscopy*

Mechanically undisturbed specimens, extracted from the water saturated samples in the oedometers, were freeze-dried and trimmed to a size of a few cubic millimeters for saturation with a monomer mixture of 85 % butyl methacrylate and 15 methylacrylate to which 2 % EWM catalyst (2.4-dichlorbenzoylperoxide) was added. After polymerization 300 to 500 Å sections were prepared for the electron miscroscopy, the ultra-microtomy being made by Eva Hanson, Dept. of Histology, Univ. of Lund.

Clay samples prepared from material originating from the two levels 0.7 and 4.7 m below the clay/rock interface were investigated with respect to the general microstructural organization and the occurrence of cementing agents. The ultramicrotomy of the 0.7 m sample offered considerable difficulties in obtaining sufficiently large, intact sections and this indicated the presence of cementing substances. Although the microstructure represents artificially produced clays, the optical microscopy shows it to be valid also of the natural clay.

Fig.7 shows typical overview micrographs of samples of the two investigated levels. The wavy pattern of montmorillonite stacks is obvious on this scale in both clays but it is clear that the upper, heated clay is less "dispersed" and that its particle network forms dense, continuous branches with larger voids between than in the unheated clay. The heated clay also has a higher frequency of isolated crystals of opaque minerals which are integrated in the smectite network and which may have resulted from the heating period. The whole pattern of this clay is very similar to that of montmorillonite clay that has been heated to 150^{o}C or more for a few weeks under hydrothermal conditions with respect to the distribution of the smectite stacks and to the presence of nodular precipitations (2).

The different microstructural character of the heated and unheated parts of the clay stratum is even more obvious at higher magnifications. Thus, Fig.8 demonstrates the denser particle grouping in the clay from 0.7 m distance below the clay/rock interface and it also clearly reveals the presence of nodules with a size of 0.01 to 0.05 microns which are assumed to be silica precipitates formed at the cooling.

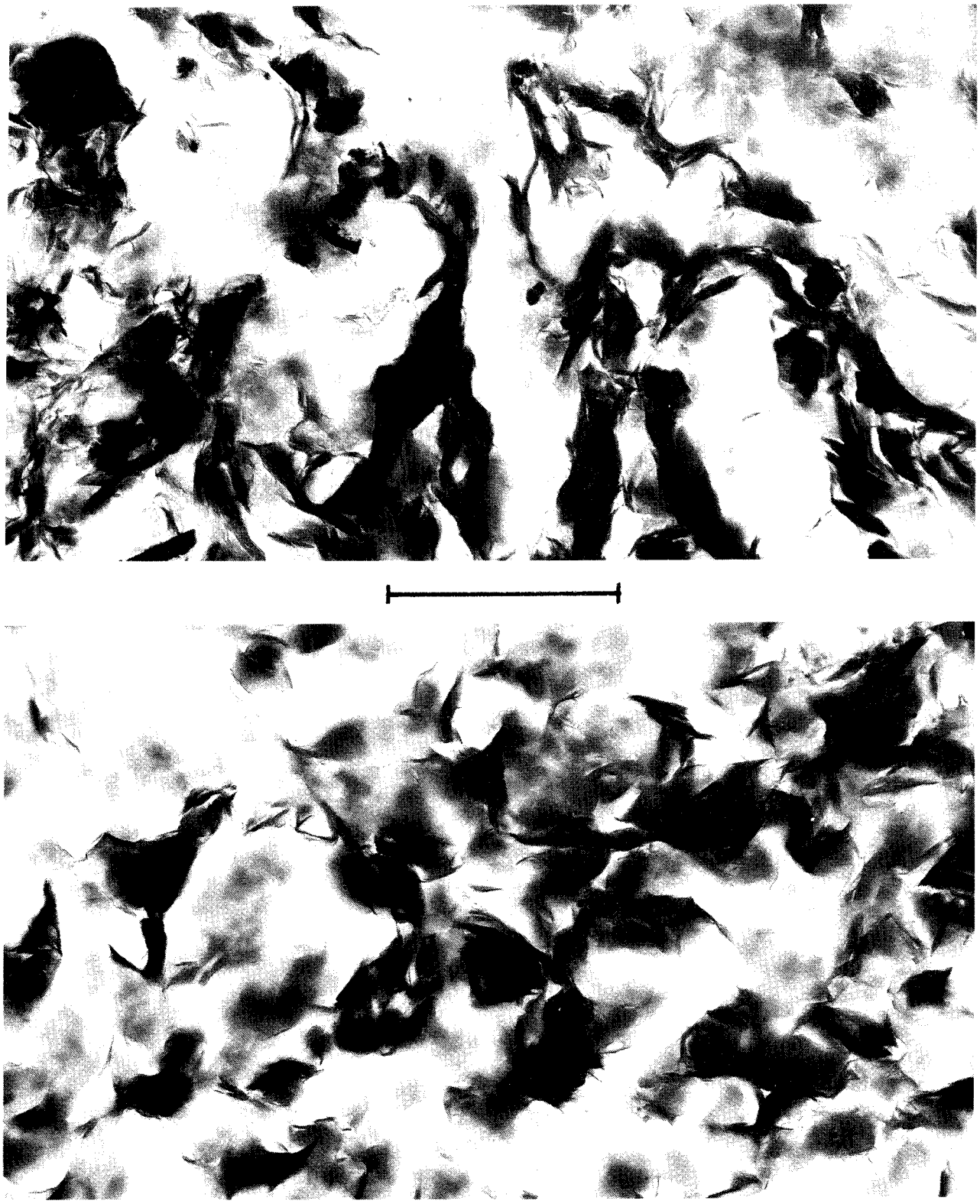

Fig.7. Electron micrographs of the clays prepared from material extracted 0.7 m (upper), and 4.7 m (lower) below the clay/rock interface. Notice the much denser particle branches and larger continuous voids in the upper picture. Scale is 1 micron

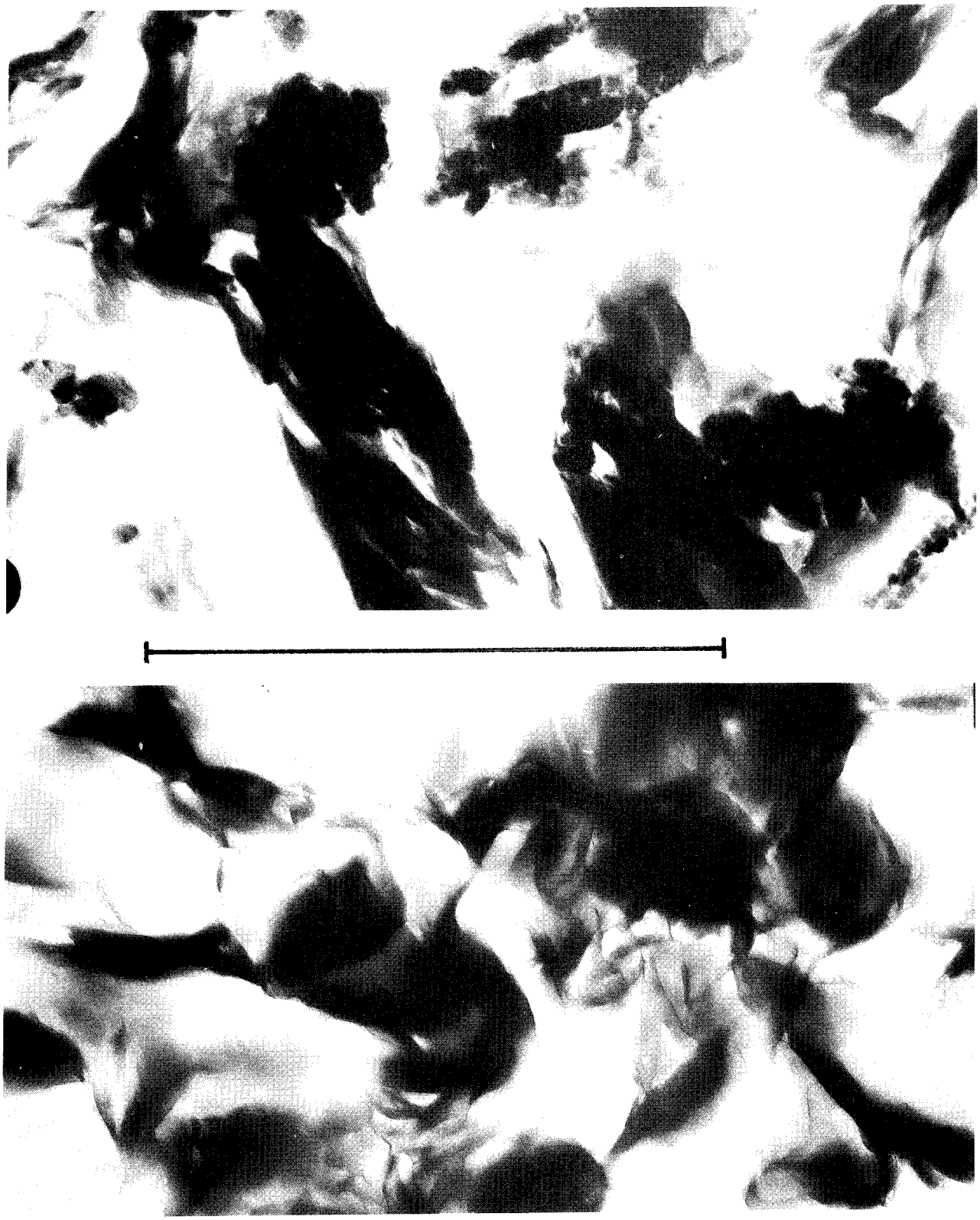

Fig.8. Electron micrographs of higher magnification of the clays prepared from material extracted 0.7 m (upper), and 4.7 m (lower) below the clay/rock interface. Notice the "collapsed" stacks and the nodules in the upper picture. Scale is 1 micron

Fig.9 illustrates additional features that can be identified at even higher magnification. It can be seen that the unheated and heated clays both contain particles smaller than 0.05 microns but while they frequently appear to be electron-transparent clay phyllosilicates in the unheated clay material, they are usually opaque nodular objects in the heated material.

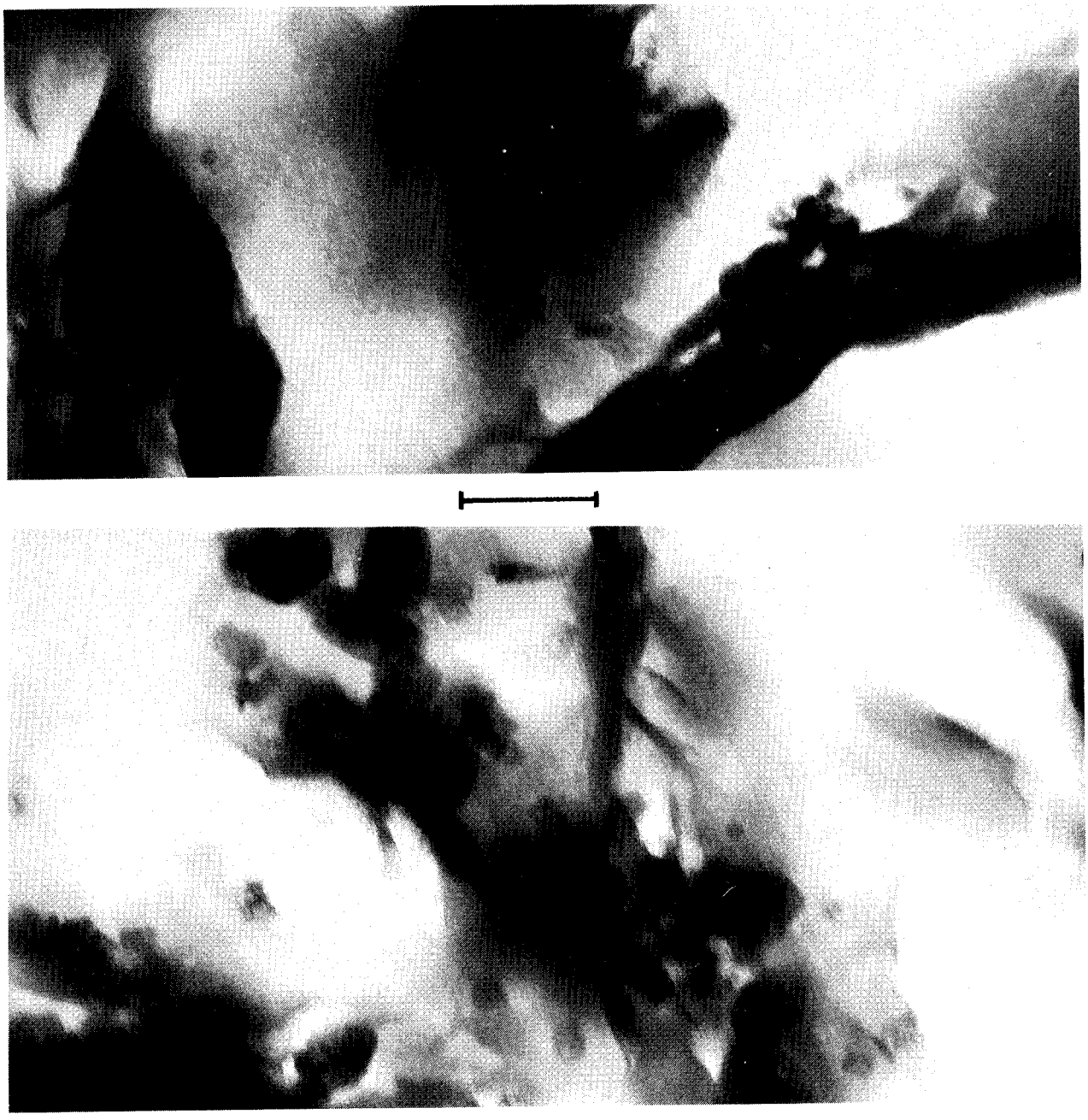

Fig.9. Electron micrographs showing very small opaque, nodular objects in the heated material (upper), and minute phyllosilicate particles in the unheated material (lower). Scale is 0.1 micron

2.1.4 Geotechnical properties

2.1.4.1 *Swelling pressure, hydraulic conductivity*

The hydraulic conductivity, swelling pressure, and rheological behavior were determined by using samples prepared from dry clay powder that was applied, compacted, and saturated with distilled water in swelling pressure oedometers. The reason for using distilled water was that it was not clear at that instant whether sodium formed a significant part of the adsorbed ions, in which case saturation with Forsmark water would have interfered with the colloid chemistry of the system.

The dry density was chosen to be 1.25 g/cm^3, corresponding to a bulk density and water content of the saturated sample of 1.8 g/cm^3 and 38 %, respectively. This density is assumed to be slightly higher than the *in situ* density since the corresponding swelling pressure exceeds the present overburden pressure. The swelling pressure and hydraulic conductivity of two characteristic samples, i.e. those from 0.7 and 4.7 m depth, were determined (cf. Table 5).

Table 5. Swelling pressure and hydraulic conductivity of Busachi clay samples

Depth below clay/rock interface, m	Swelling pressure MPa	Hydraulic conductivity m/s
0.7	0.48	3×10^{-11}
4.7	0.51	10^{-11}

The small difference in swelling pressure and hydraulic conduct between the two samples supports the conclusion from the mineralogical study that the smectite contents are not very different. However, the three times higher permeability of the shallow sample is well explained by the the more porous microstructure of the heated clay. It is interesting to

see that the properties of the Busachi clay series are similar to those of other smectite-rich clays. Thus, at a bulk density of 1.8 g/cm^3 a typical value of the swelling pressure of Ca bentonite is 0.3 MPa of Ca bentonite and 0.55 MPa of Na bentonite (MX-80), while the hydraulic conductivity of the first-mentioned is between 10^{-12} and 10^{-11} m/s, and around $5x10^{-13}$m/s of the latter.

2.1.4.2 *Rheological properties*

Creep tests were made to determine the general stress/strain/time behavior of samples from 0.7 and 4.7 m, respectively. The intention was to find out whether the indications of cementation effects in the first-mentioned, heat-effected part of the clay serie is manifested by anomalous creep properties.

Air-dry clay material was gently crushed to a fine-grained matrix which was put in a 2 cm diameter shear box and slightly compacted to yield a final bulk density of 1.8 g/cm^3 after saturation with distilled water at a normal pressure of 0.5 MPa, which remained constant throughout the creep tests. The shear stress was increased stepwise, the load steps being set at approximately 20 % of the shear strength. The angular shear strain was evaluated by applying the expression in Eq. 1, which was derived from an earlier FEM-based study of the shear stress distribution (3):

$$\gamma = \frac{3\varepsilon}{\sqrt{1-\frac{\Sigma\Delta}{\Delta f}}} \qquad (1)$$

where Δ is the recorded shear displacement for the respective load step and $\varepsilon = \Delta/D$, D being the diameter of the shear box. Δf is the total shear displacement at failure.

Each load step was left on until the angular shear strain had dropped to about 10^{-8} s^{-1} in most cases. The evaluated relationship between time, strain, and strain rate, respectively, are shown in Figs. 10 and 11.

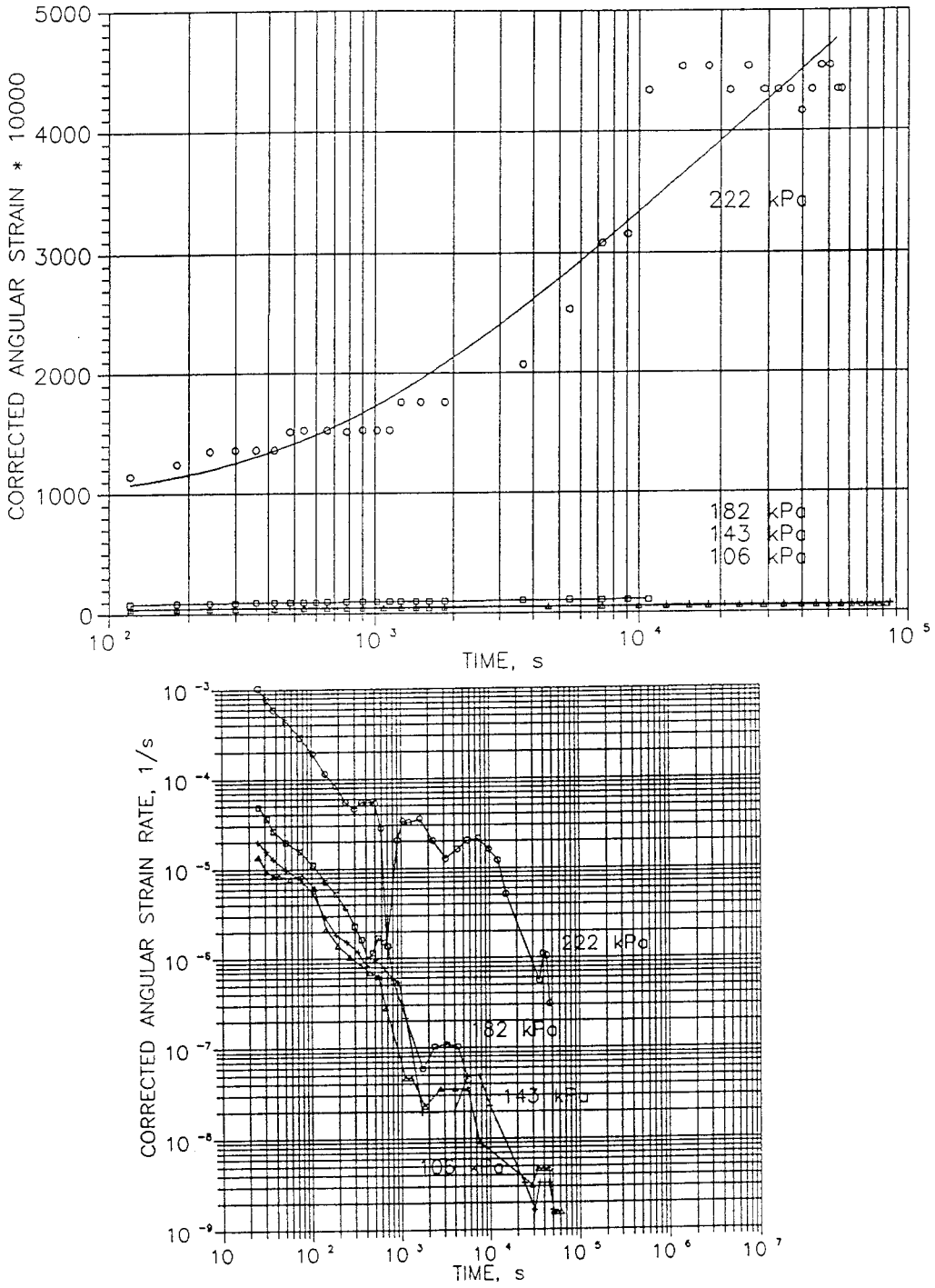

Fig. 10. Creep strain versus time (uppper), and strain rate versus time (lower) of Busachi clay from 0.7 m below the clay/rock interface

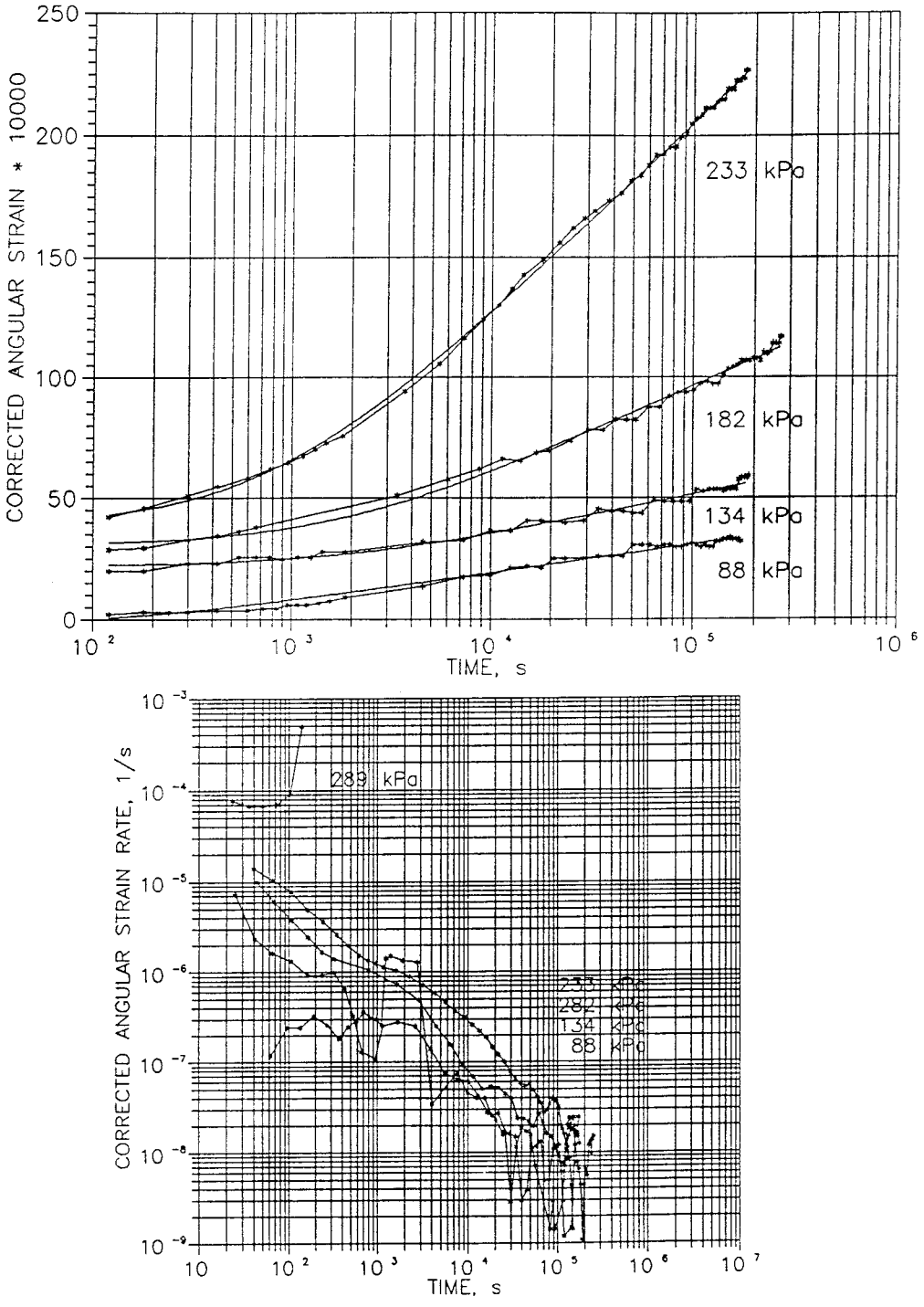

Fig. 11. Creep strain versus time (upper), and strain rate versus time (lower) of Busachi clay from 4.7 m below the clay/rock interface

The creep behavior of the sample from 0.7.m depth below the clay/rock interface is very clearly influenced by cementation effects. Thus, the upper diagram in Fig.10 demonstrates that the shear strain is very insignificant at stresses below a critical level, i.e. about 200 kPa, and that it has the jerky character that is typical of cemented clay, cf.(3). The lower diagram shows an irregular change in the rate of strain and a rapid drop at all stress levels after about 10^4 seconds, indicating that a creep law of the type:

$$\gamma = \alpha t - \beta t^2, \quad (t < \frac{\alpha}{2\beta}) \qquad (2)$$

where α and β are material constants and t is the time after onset of creep. This type of creep has been shown to be characteristic of strong, "overconsolidated" materials for which one can disregard from "softening" effects on a molecular scale. Thus, applying the modern philosophy of stochastic slip as the basic mechanism in creep, the physical model allows only for jumps which, when they take place, bring the slip units up against a barrier by a certain amount *higher* than the previous one (4).

The diagrams in Fig.10 demonstrate that the behavior of the clay from the lower level is very similar to what is usually found for non-cemented smectite-rich clays, i.e. smooth curves (upper graph), and a successive approach to log time creep. Thus, in contrast to the heated clay, the creep rate increased exponentially with the shear stress. The curves representing creep rate versus time are approximately parallel, except for the one representing the highest value, 289 kPa, which led to failure. The irregular shape of these curves after about 10^4 seconds is due to the limited accuracy of the electronic recording units. It is concluded that the creep properties of the clay from 4.7 m level below the clay/rock interface do not show any sign of being heat-affected, which is thus in agreement with the theoretically deduced temperature distribution given in Table 4.

2.1.5 Conclusions

It is clear from the mineralogical and rheological tests that the short term heating caused very small changes in the composition and properties of the clay series, except for the clay/rock contact. Here, the major effect was precipitation of heat-released substances, which caused cementation and thereby reduction of the swelling potential and development of brittle behavior.

The non-expanding minerals formed in the partial transformation of the montmorillonite content in the clay/rock contact zone may be hydrous mica of the illite type but it may very well be a matter of montmorillonite, collapsed to 10 Å by the heating and then prevented from expanding by the cementing agents. Precipitation of small nodules, interpreted as silica precipitations at the edges of montmorillonite stacks, is actually in support of this hypothesis.

2.2 Gotland bentonite

2.2.1 Geological history

The bentonite bed at Hamra, southern Gotland (Fig. 11), is assumed to be of Ordovician age. The rocks exposed on Gotland consist of Silurian deposits, which cover Ordovician and Cambrian sediments resting on crystalline bedrock at about 525 m depth at Hamra. Bentonite layers of various thickness, usually only a few centimeters thick, occur throughout the Ordovician series and they all stem from eruptions of volcanic ash that was sedimented in the salt sea that covered the area at that time. The 0.3 m thick bed, which will be described in this report, is located at 515 m depth and may have the same origin as the 2 m thick bed at Kinnekulle. The rest of the sediment series at Hamra is dominated by marly limestone and relatively pure, crystalline limestone. The general lithology of Gotland is shown in Fig. 12.

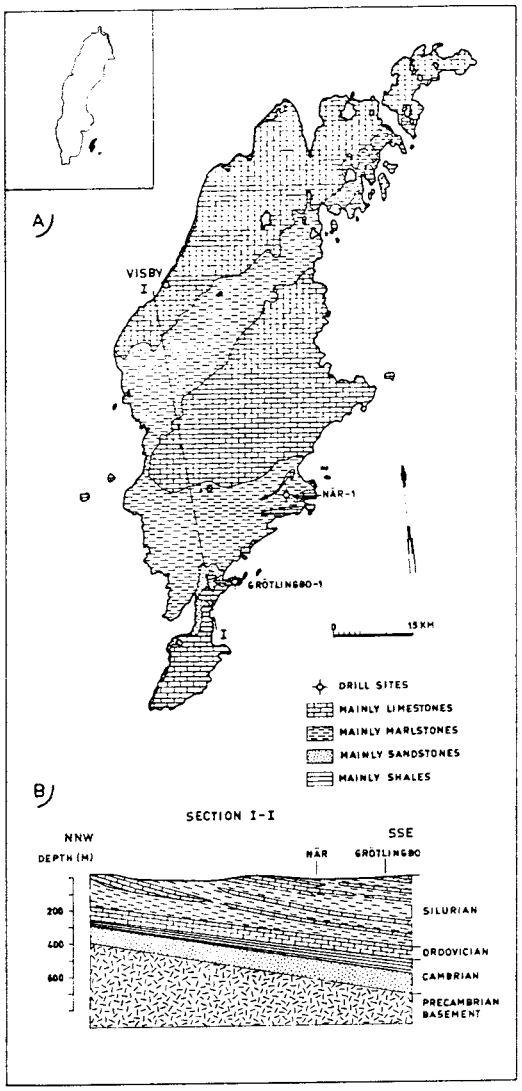

Fig. 12. Location of Hamra, and stratigraphic profile of Gotland (Snäll)

There are no obvious signs of eruptive events or large tectonic disturbances associated with percolation of hydrothermal solutions and no diabase intrusions have been found. Still, there are two indications of rather severe movements in the earth crust that may have caused local heating of the sediments in southern Gotland. One is the conclusion by Agterberg from his study of the large-scale stratigraphy of southern Gotland, that the Burgsvik and Hamra strata wedge out in opposite directions and that this can be explained by a moving descent during their formation (5). He assumed that when the sand - now forming the Silurian sandstone series exposed along the coastline between Burgsvik and Hoburgen - was deposited, the basin descended strongest in the west, near to the coast of that time, while in course of time this belt moved eastward, so that the sandstone is thinner there and covered by a thicker Hamra Limestone. Agterberg supposed that the moving descent was caused by a flow of magma that could not escape upwards, the flow being associated with the Caledonian orogenesis. This would imply much higher temperatures than those indicated by the present thermal gradient, particularly of the lower parts of the Ordovician series, during very significant periods of time, probably many hundred thousands or even millions of years.

A second indication of strong heating of the sediments is the recording of geophysical anomalies, indicating post-Ordovician granitic domes in the Hamra area (pers. comm. Fred Linder, OPAB). However, while neither of these indications offer any real evidence of the absolute temperatures or the heating history, the heating can be rather accurately determined by considering mineralogical data and by applying reasonable thermal gradients as will be shown in the subsequent text. All this has led to an unanimous picture of the pre-existence of at least 2 km of Devonian sediments that were later removed by erosion. It is therefore concluded that the Ordovician bentonite bed was covered by about 2.5 km of sediments, which caused an effective vertical pressure of at least 30 MPa. This pressure condition and the associated elevated temperature state must have prevailed for tens of millions of years and probably longer than that.

A matter of great importance in evaluating the mineralogical evolution is the chemical composition of the salt sea that covered the area in Ordovician time, particularly with respect to the potassium concentration. The fact that glauconite is richly represented in certain Paleozoic strata may actually indicate a higher potassium content in certain periods, but although it is not unrealistic to envisage conditions of large peneplain exposure to weathering that may have led to a significantly higher K/Na ratio than at present, we will make the conservative assumption here that the ancient sea water had the same chemical composition as the present oceans. It is clear that temperate conditions prevailed in the large sea that covered the area in Ordovician time (pers. comm. Prof. Valdar Jaanusson).

2.2.2 Temperature history

2.2.2.1 *Pressure solution in the Silurian Burgsvik sandstone*

Sandstone samples from the Kättelviken area north of Hoburgen, southern Gotland, were investigated by the senior author almost 20 years ago with the purpose of estimating the preconsolidation pressure of the Silurian clay beds in the area. The study comprised visual inspection of thin sections in order to identify the nature of the grain contacts for evaluation of the thickness of pre-existing, overlying sediments by use of the diagram in Fig. 13, which shows empirically stress-correlated contact types in sandstone (6).

A common feature is that many grains are coated by precipitated carbonates and this process appears to have taken place rather early in the sedimentation process such that stress transfer took place through the intergrown cementing coatings of many neighboring grains. However, there is a sufficient number of direct contacts between quartz grains to allow for stress evaluation (Fig. 14). One finds that the most interfingered contacts represent slightly more than 20 % of all contacts, while the single-penetration type represents about 20 - 25 %, and flat-contact type represent about 50 % . For this constellation the

diagram suggests that the overburden has been in the range of 2000 to 2400 m. Since the Ordovician bentonite bed is located about 500 m deeper down, this study shows that the bed has been covered by 2.5 to 3 km of sediments, of which the upper 2 - 2.5 km were of Devonian age.

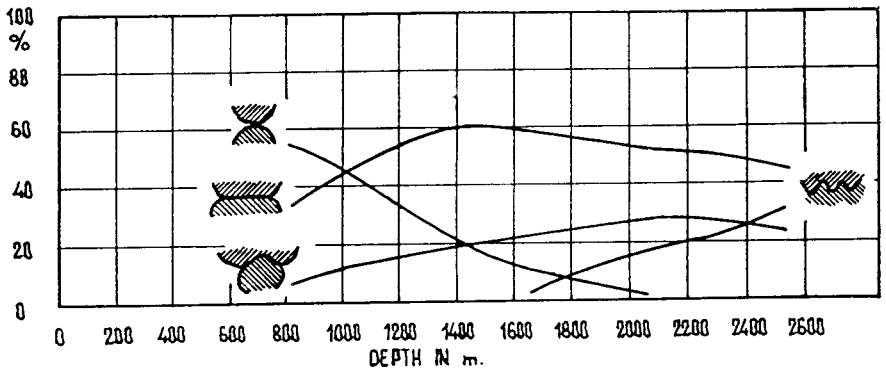

Fig. 13. Empirical relationship between the thickness of sediment overburden and the frequency of different types of grain contacts

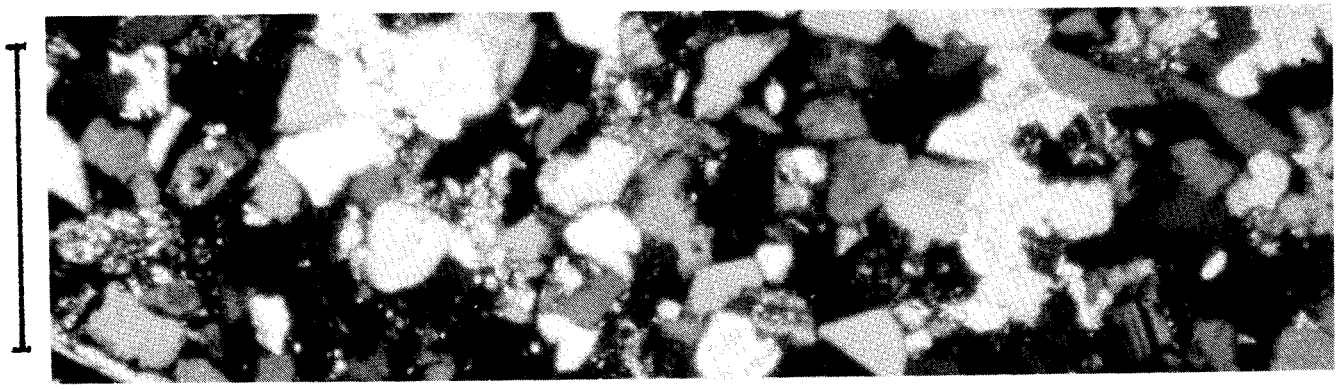

Fig. 14. Example of grain contacts in the Silurian sandstone presently exposed in the Burgsvik area. Scale is 1 mm

2.2.2.2 *Thermal alteration of organic constituents*

Determination of the thermal alteration index of kerogene has yielded values from which one can safely conclude that the bentonite bed has been exposed to 90 - 100°C for tens of millions of years (Pers. comm. Fred Linder, OPAB). Back-calculation using the thermal gradient 27°C suggested by OPAB, yields a total overburden of 2.8 km, i.e. well in the range derived from the pressure solution study. The thermal alteration study is, however, said to indicate a stronger change in color in the southern direction, indicating that the thermal gradient has been higher in the southernmost parts of Gotland. This is in agreement with other data reported from Gotland (7), showing that the present gradient is locally as high as 47°C/km.

2.2.2.3 *Mixed layer minerals as paleotemperature indicator*

Evaluation by Dr Sven Snäll, SGU, of the ordering of smectite and illite flakes in samples extracted from Grötlingbo, located 20 km northeast of Hamra has given further information on the temperature history (8,9). Snäll made use of the following basic conclusions from comprehensive studies in the field of paleotemperature indicators:

* At depths smaller than 0.5 km and temperatures below 100°C smectites remain stable

* With pure smectites as initial dominant constituents in deeply buried clays, irregularly sandwiched clays I/S is characteristic of the first alteration phase. An I/S ratio of 50/50 is representative of this first stage, while the second stage involves the establishment of a certain I/S order, with illite forming 50 - 80 % of the total mass ("allevardite"). This stage is reached at 90 - 110°C at more than 3 km depth, while at 1 km depth, the temperature may have to be as high as 180°C. "Kalkberg", formed at 180 - 210°C at larger depths than 1 km, is the term of the third

stage, which is taken to have 3 illite sheets interlayered with 1 smectite sheet as a typical feature. At smaller depths illite and chlorite are formed instead. In the fourth stage, finally, all smectite is replaced by illite.

* Temperatures indicated by the mineral compositions represent the *maximum* heating level. Subsequent, significant drops in temperature and pressure give negligible further changes, since retrograde processes are concluded to be extremely slow.

* The influence of kinetics is considerable at temperatures below 100°C but it is insignificant in the range of 100 - 200°C, referring to Velde.

* The initiation of the third stage coincides with the lower boundary of the temperature range in which liquid hydrocarbons appear, i.e. at 90 - 110°C.

Using these mineral/temperature correlations, Snäll concluded from his XRD analyses (9) that the allevardite-type material, which was dominant in the Grötlingboudd samples from 100 - 450 m depth, can have been formed at smaller depths than 1 km if the temperature exceeded 170°C, while the temperature must have been at least 110°C if the depth was 2.5 km.

Snäll investigated this matter further by determining the crystallization index (CI), the sharpness ratio and additional XRD features of illite extracted from the cores, and concluded from these data as well as from the occurence of oil traces, that the alteration of the sediments is within the "oil window", and that the bentonite layers have been exposed to prolonged heating to 120°C.

It should be added that Snäll found through his studies that the major adsorbed cation in the clays is Ca and that the smectite component is of the montmorillonite type.

2.2.2.4 *Conclusions*

It is concluded from the various sources referred to in the preceding text that the Hamra bentonite bed that is presently located at 515 m depth has been exposed to 110 - 120°C for at least 10 million years. Applying a thermal gradient of 30°C/km and 3 km overburden one would get the figure 110°C, assuming the ground temperature to be 20°C. Using, for comparison, recent data from the Ekofisk area in the North Sea, where the temperature is 130 - 135°C at 3090 m depth, one concludes that the temperature was slightly higher than 110°C at Hamra and that Snäll's value 120°C appears to be more correct. We will see later that this would also give very good agreement between the mineral compositions. In the North Sea, one finds that shales contain a separate smectite phase at a maximum temperature of 115°C, and that only mixed-layer I/S and a separate illite phase are present at 125 °- 150°C (Pers. comm. Dr Knut Pederstad, Norsk Hydro, Stabekk).

2.2.3 General properties

OPAB's core description used the term "light green, soft waxy with large phlogopite flakes" for the clay as it appeared at the drilling about 10 years ago. The thickness of the bed from which the samples originated was about 30 cm.

2.2.3.1 *Grain size distribution*

The core samples, which appeared to be homogeneous but still characterized by slight lamination, were prepared for the granulometrical investigation by sieving, drying at 105°C and dispersing in distilled water with sodium pyrophosphate by applying ultrasonic treatment. By this, complete disintegration occurred, indicating that cementation effects were absent or very minor. The grain size distribution is illustrated in Table 6, from which one concludes that the clay content is very high.

Table 6. Granulometry of the Hamra bentonite

Equivalent Stoke diameter d, mm	Weight percentage of material finer than d
0.04	98
0.02	94
0.01	92
0.006	90
0.002	87

2.2.3.2 *Chemical data*

The chemical composition of the clay was determined by the Swedish Geological Co, Luleå, by applying plasma technique (ICP-AES) after dissolution in lithium borate. Table 7 gives the main elements, while the major trace elements were barium (891 ppm), zirconium (564 ppm), strontium (211 ppm), and lantane (100 ppm). It is concluded that the potassium content is remarkably high while the content of calcium is surprisingly low, considering the marl-type environment.

Table 7. Chemical composition of the Hamra bentonite

Element	Concentration
SiO_2	54.8 %
Al_2O_3	22.9 %
Fe_2O_3	2.9 %
MnO	0.0 %
TiO_2	0.3 %
MgO	4.0 %
CaO	0.9 %
K_2O	5.8 %
Na_2O	0.6 %
P_2O_5	0.1 %
H_2O	6.4 %

2.2.3.3 *Geotechnical data*

The core samples originated from a storage which had caused partial drying to a water content of about 10 % without fracturing or fissuring. After water saturation in a shear box without allowing for any expansion, the bulk density was 2.12 t/m^3 and the water content 19 % .

The liquid limit was found to be 76 %, indicating a fair amount of smectitic minerals. Thus, with Ca in exchange positions, which would be plausible with respect to the rich representation of marls in the Ordovician sediments, one would expect a liquid limit of about 100 % if the clay fraction holds about 90 % montmorillonite, and about 50 - 60 % if it has that amount of illite. It is concluded that smectites form 30 - 60 % of the clay fraction.

2.2.3.4 *Mineralogical data*

The cation exchange capacity was determined and two types of XRD analyses were conducted in order to characterize the Hamra bentonite with respect to the mineralogy. Additional information was offered by the microstructural investigation reported in the subsequent chapter.

The cation exchange capacity was determined by the Swedish Geological Survey, applying the following procedure. 8 g of clay, representing the clay fraction, were dispersed in 100 ml of $SrCl_2$ solution and mechanically agitated for 24 hours. The clay was then washed with distilled water and 70 % alcohol solution 7 times. After drying at 105°C the strontium content was determined and the cation exchange capacity evaluated as 36 meq/100 g. This supports the conclusion from the determination of the liquid limit that the smectite content is in the range of 30 - 60 % .

The XRD determination was made both by the Swedish Geological Survey and by the Swedish Geological Co in cooperation with the Dept. of Chemistry, University of Lund. Oriented minus 2 micron specimens were used for the analyses.

A first attempt in using XRD was to apply Reynolds' method for quantifying the content of montmorillonite, using pyrophyllite as a reference substance. The procedure was the same as that used for the Busachi clay series, the evaluated parameter values being given in Table 8. A typical diffractogram of EG-treated clay is shown in Fig. 15.

Table 8. Parameters obtained by applying Reynolds' method (Erlström)

Mineral	Reflection	Intensity	MIF	1/MIF	%
Pyrophyll. (reference)	002	37.5	0.6	62.5	5
Hydr. mica (10 Å min)	003	412	1.0	412	
Montmorill.	005	812	1.06	766	95

The evaluated montmorillonite content from the parameter values given in Table 8 was 66 %, while the content of hydrous mica would form the remainder, i.e. 34 % . The values refer to the phyllosilicate minerals of the clay fraction and since there are also some rock-forming minerals like quartz, feldspars and heavy minerals and micas, the actual content of montmorillonite in the clay fraction is estimated at about 40 to 50 % .

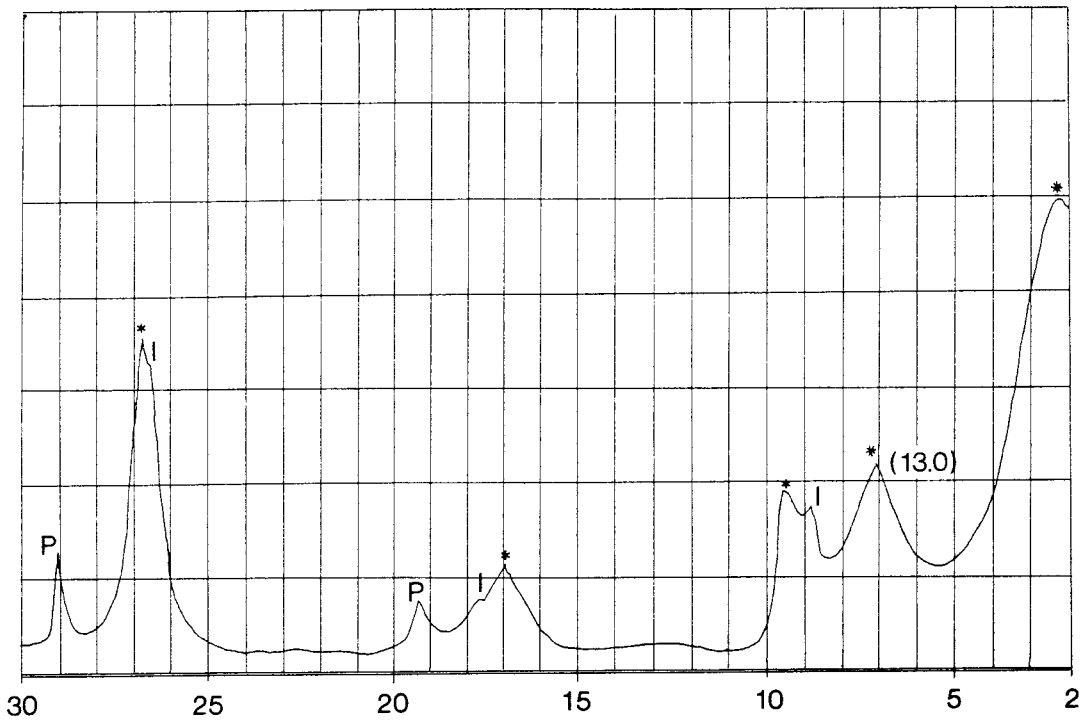

Fig. 15. XRD diagram of EG-treated material from the clay fraction of the Hamra bed. Bottom figures give 2Θ. P denotes pyrophyllite added.

* = from right to left: first, second, third, fifth and eigth order of reflection in the 27 Å basal spacing of the I/S mixed layer component.

I = from right to left: first, second and third order of reflection in the 10 Å basal spacing of the discrete illite.

A second attempt was made to identify the clay mineral constituents of the clay fraction by examining the XRD/EG diffractogram and applying Fourier analysis for distinguishing between 10 Å minerals (termed "illite", i.e. I, here), and smectite. The obvious reason for this was the presence of the rather broad peak corresponding to d = 13 Å, which indicates relatively ordered I/S stacking. For that purpose Reynold's computer program NEWMOD was used for the calculation of one-dimensional X-ray diffraction patterns of mixed-layered clays. The intention of the study was to find out what the actual spectrum of possible combination

of stacking orders really may be, and to correlate these orders with the microstructural patterns shown by electron microscopy. After an initial, overview study three reasonably possible combinations were looked at, all implying that Ca is in the exchange positions of the smectite phase:

1. Completely segregated I and S phases
2. Mixed layering of I/S with different degrees of ordering
3. Mixed layering of S and other 10 Å minerals than I

Case 1

The synthetic diffractogram (Fig. 16) is completely different from the actual XRD/EG diagram in Fig. 15. A safe conclusion is therefore that a significant part of the clay minerals occur in some kind of integrated pattern characterized by stacking.

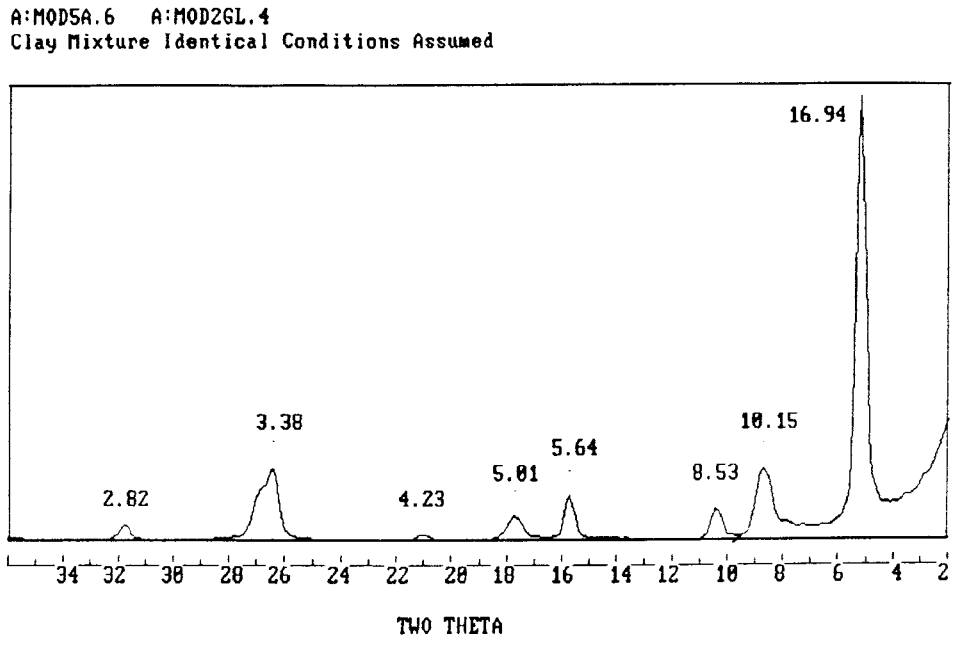

Fig. 16 Synthetic XRD/EG diagram for completely segregated I/S. Bottom figures give 2Θ in this and subsequent diagrams

Case 2

The I/S mixed-layer type stacking is of particular interest since such a system was concluded to be at hand in the Grötlingbo core earlier investigated by Snäll (9). A basic condition of such systems is that the maximum basal plane distance is about 27 Å and the dominating peaks of the synthetic diffractograms relate to the 1st, 2nd, and 3rd order reflections of this distance. Thus, the 13 Å peak of the true diagram represents the second order reflection of the 27 Å distance.

The agreement between the synthetic mixed-layer patterns and the true one in Fig. 15 is bad for random gropings, i.e. with "Reichweite" = 0, as demonstrated by Fig. 17, but the fit is rather good at higher degrees of ordering (Fig. 18 with Reichweite = 1, and Fig. 19 with Reichweite = 0.5). Reichweite = 1 represents completely regular ordering with each S-flake followed by an I-flake, while Reichweite = 0.5 means an intermediate condition between completely random and completely ordered arrangements.

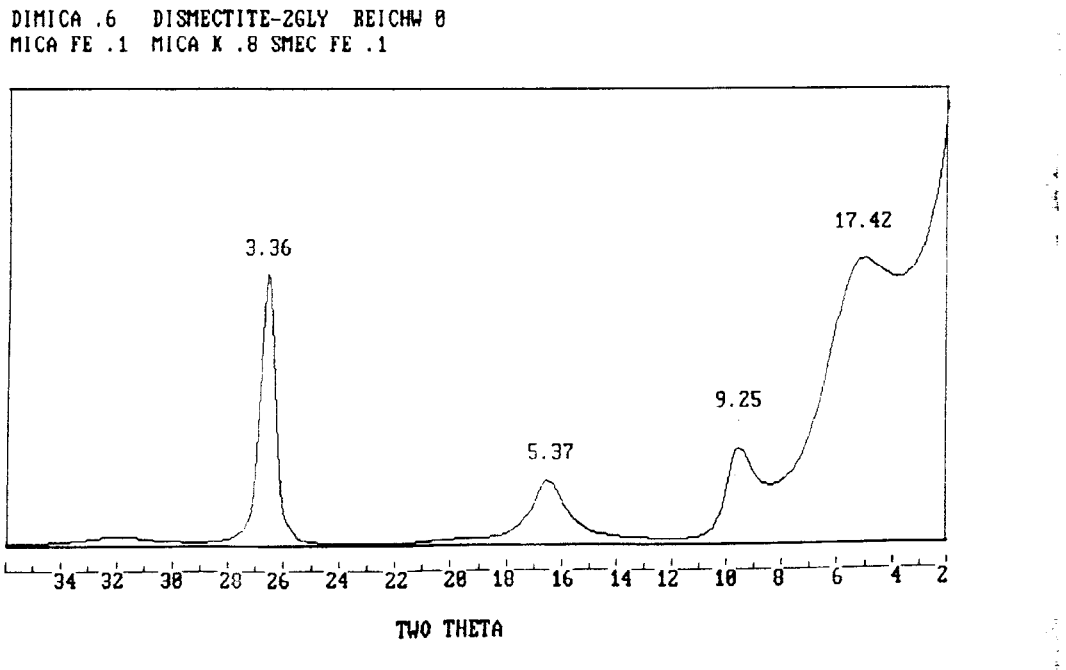

Fig. 17. Synthetic XRD/EG diagram for mixed-layer I/S with Reichweite 0

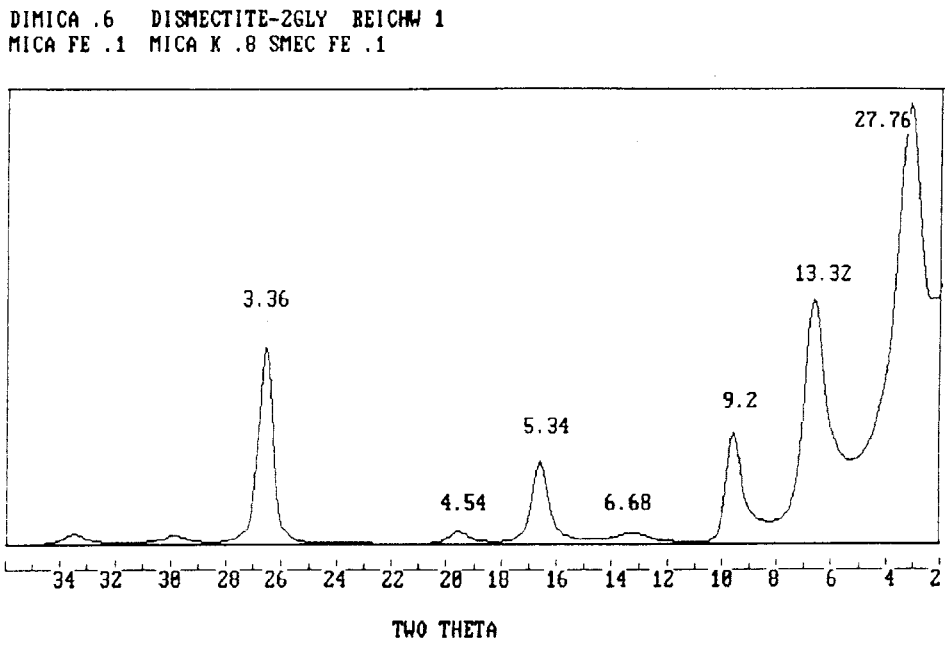

Fig. 18. Synthetic XRD/EG diagram for mixed-layer I/S with Reichweite 1

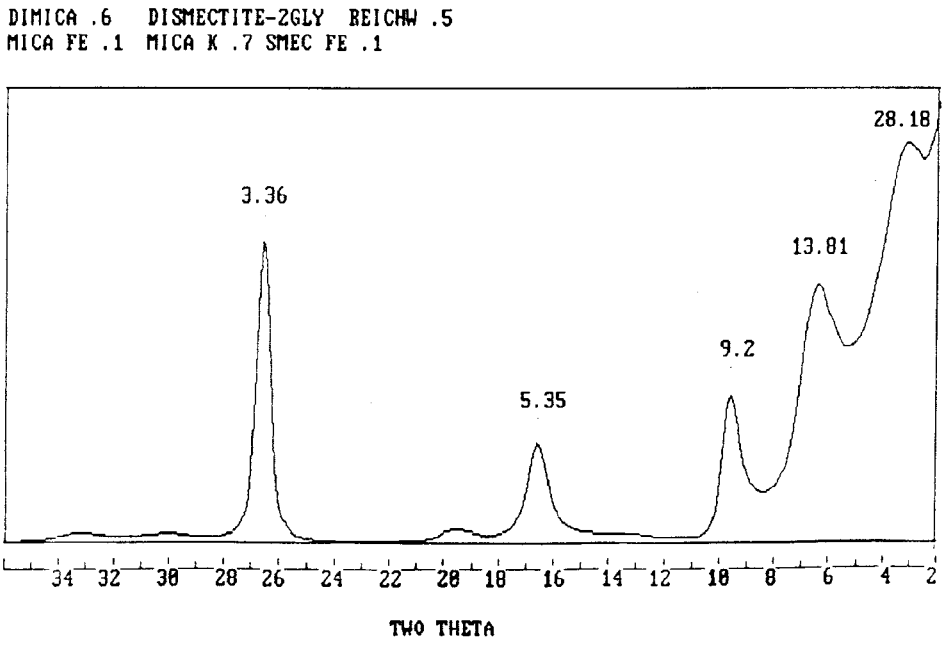

Fig. 19. Synthetic XRD/EG diagram for mixed-layer I/S with Reichweite 0.5

Case 3

Reynolds' computer program is based on the implication that, for illite, 0.5 Si atoms out of 4 tetrahedrally located ones are replaced by Al, and that 0.3 Al atoms out of 2 octahedrally hosted ones are substituted by Mg. The entire resulting charge deficit (i.e. 0.8 per 0.5 unit cell) is assumed to be compensated for by potassium, thereby creating the I phase as represented by the synthetic diffractograms in Figs. 16 - 19.

The program does not allow for introduction of other interlamellar cations than potassium but it is still possible to simulate alternatives to illite, such as brammalite or the corresponding equivalent with locked-in calcium, by manipulating the number of cations per 0.5 unit cell. Thus, assuming that calcium is present in stead of potassium, still with the same charge deficit of 0.8 per 0.5 unit cell, one can simulate the calcium case by taking 0.4 potassium ions instead of the actually required number 0.8 (different valences, almost the same number of electrons). Correspondingly, the sodium case can be taken to be the same as that of calcium since, as compared to potassium, the valence is the same while the total number of electrons is about 50 % .

The diffractogram in Fig. 20 was obtained by applying Reynolds' program, assuming that sodium or calcium is in interlamellar positions of the hydrous mica and that the Reichwerte is 0.5. The remarkable fact is that it cannot be distinguished from the illite case in Fig. 19, which means that the identification of the type of hydrous mica in mixed-layer minerals assemblages may be very uncertain. Theoretically, at least, the Hamra clay fraction may thus be characterized by a moderately well ordered stacking of montmorillonite and hydrous mica with potassium, sodium or calcium fixed in the interlamellar positions of the latter component. The high K-content of the clay would suggest that the hydrous mica is actually illite but we will demonstrate later that it is most probably related to a separate illite phase.

Additional

The capacity of the program is sufficient to manage also other minerals added to the mixed-layer material in any proportions. Such

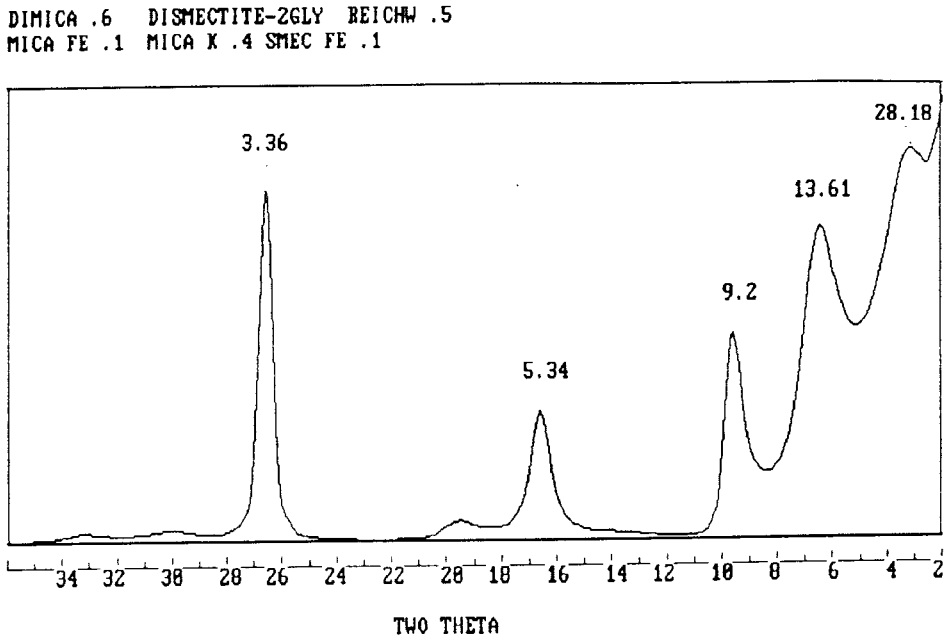

Fig.20 Synthetic XRD/EG diagram for mixed-layer montmorillonite/hydrous mica with Na or Ca fixed in the interlamellar space of the latter component

addition does not yield any new mixed-layer components but simply represents a physical mixture of the constituents. Considering the peak at about 9 Å of the true diffractogram in Fig.15, it is logical to assume that it is affected by a segregated 10 Å mineral phase. Using the program to yield synthetic diffractograms with pure illite added, and with illite and pyrophyllite added as represented by Fig.15, one obtains the diffractograms in Fig.21 and Fig.22 from those in Fig.19 and Fig.20, respectively. The combinations are thus:

A. 70 % mixed-layer I/S with K fixed in the hydrous mica +
20 % pure illite + 10 % pyrophyllite (Fig.21)

B. 70 % mixed-layer I/S with Na or Ca in the hydrous mica + 20 % pure illite + 10 % pyrophyllite (Fig.22)

In both cases the smectite content of the mixed-layer component was taken as 40 % . We find that both diffractograms are in reasonable agreement with the true one in Fig.15 and this is also the case when the smectite content of the mixed-layer component is increased to 50 % . Higher concentrations of smectite than 50 % appear to give less good agreement. The potassium content may hence be related to the separate illite phase in which case the Hamra clay is of type B with a smectite content of the mixed-layer material of 40 - 50 % . As to the major cation adsorbed in the smectite, which is presumably montmorillonite, Snäll's conclusion from the Grötlingbo study appears to be valid, meaning that Ca is in the exchange positions of the montmorillonite. Since pyrophyllite is not present in the natural clay its clay fraction is concluded to consist of 75 % mixed layer material with 40 - 50 % montmorillonite, and 25 % pure illite.

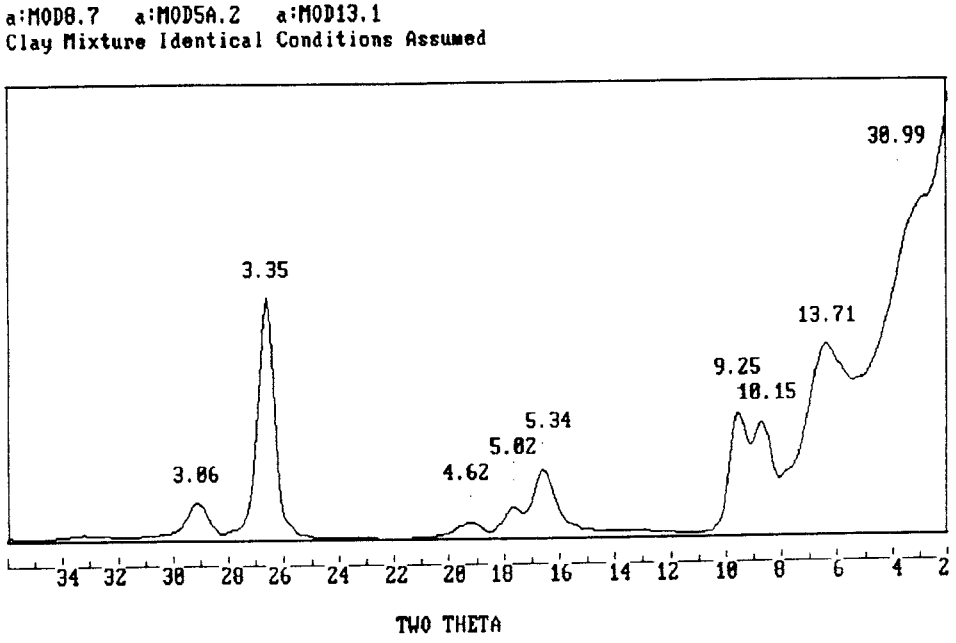

Fig.21. Synthetic XRD/EG diagram for 70 % I/S with K in the hydrous mica + 20 % pure illite + 10 % pyrophyllite. Smectite forms 40 % of the mixed-layer material

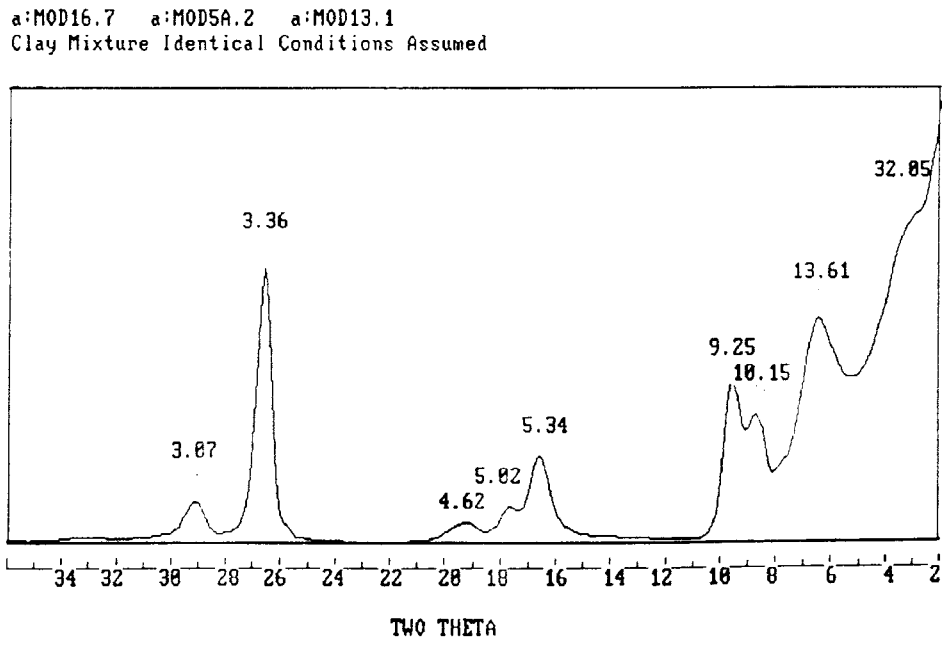

Fig.22. Synthetic XRD/EG diagram for 70 % I/S with Na or Ca in the hydrous mica + 20 % pure illite + 10 % pyrophyllite. Smectite forms 40 % of the mixed-layer material

2.2.4 Microstructural constitution

Samples were prepared for transmission electron microscopy using the same technique as for the investigation of the Busachi clay with the exception that the Hamra clay samples were mechanically undisturbed. No difficulties appeared in the ultramicrotomy, which indicates that cementation was weak or absent.

Fig.23 shows a typical overview micrograph of the Hamra clay with its homogeneous character. There is a clear trend of orientation of the I/S stacks (dark objects) inherited from the heavy overburden pressure, the general pattern being of the wavy type that is typical of smectitic

clays. The lower micrograph is characteristic of unheated Ca montmorillonite (Bavarian, Cretaceous), prepared in the same way as the Busachi samples to yield the same density as the Hamra clay (2.1 g/cm^3). We see that this clay, like the one prepared from the unheated part of the Busachi series, is more homogeneous than the Hamra clay but both exhibit similar microstructural patterns. The special feature of heated smectite clay, i.e. that of dense stacks forming a more or less continuous network, is particularly obvious in Fig.24, which also shows that illite occurs as a separate phase in larger voids. This mineral component is the 25 % pure illite identified by use of Reynolds' code, and its origin is very probably neoformation by crystallization of elements released by thermally induced dissolution of smectite in the porewater.

A close-up of the illite-rich parts of the specimens (Fig.25) exhibits well crystallized thin flakes forming a rather soft gel of this type of mineral. It is logical to believe that although the gel fills up large parts of the voids its hydraulic conductivity is probably not very low. It should be pointed out in this context that the minute illite crystallites do not form smectite-like stacks in the Hamra clay and do therefore not contribute to the swelling power of the bulk clay.

Microstructures and elemental compositions of ultramicrotomed specimens were studied by a Philips EM 400 T microscope equipped with and Link EDX 10000 X-ray and Image analyzer with the particular intention to find out the distribution of potassium in the clay, which should be confined to the dense stacks if the illitization had caused only mixed-layer I/S minerals. Analyses with respect to the distributionof Si, Al, Mg and Ca were also included in the study, which was made in cooperation with Reine Lindwall, Linköping University.

Fig.26 shows the "image" of a typical area that was selected for elemental analysis. As expected, Si and Al were uniformly distributed over the particle network, confirming that only phyllosilicate particles were present. Also K was found to have approximately the same distribution but the area mapping was not sufficiently detailed to give evidence of whether potassium was present both in the stacks and in the illite clay matrix.

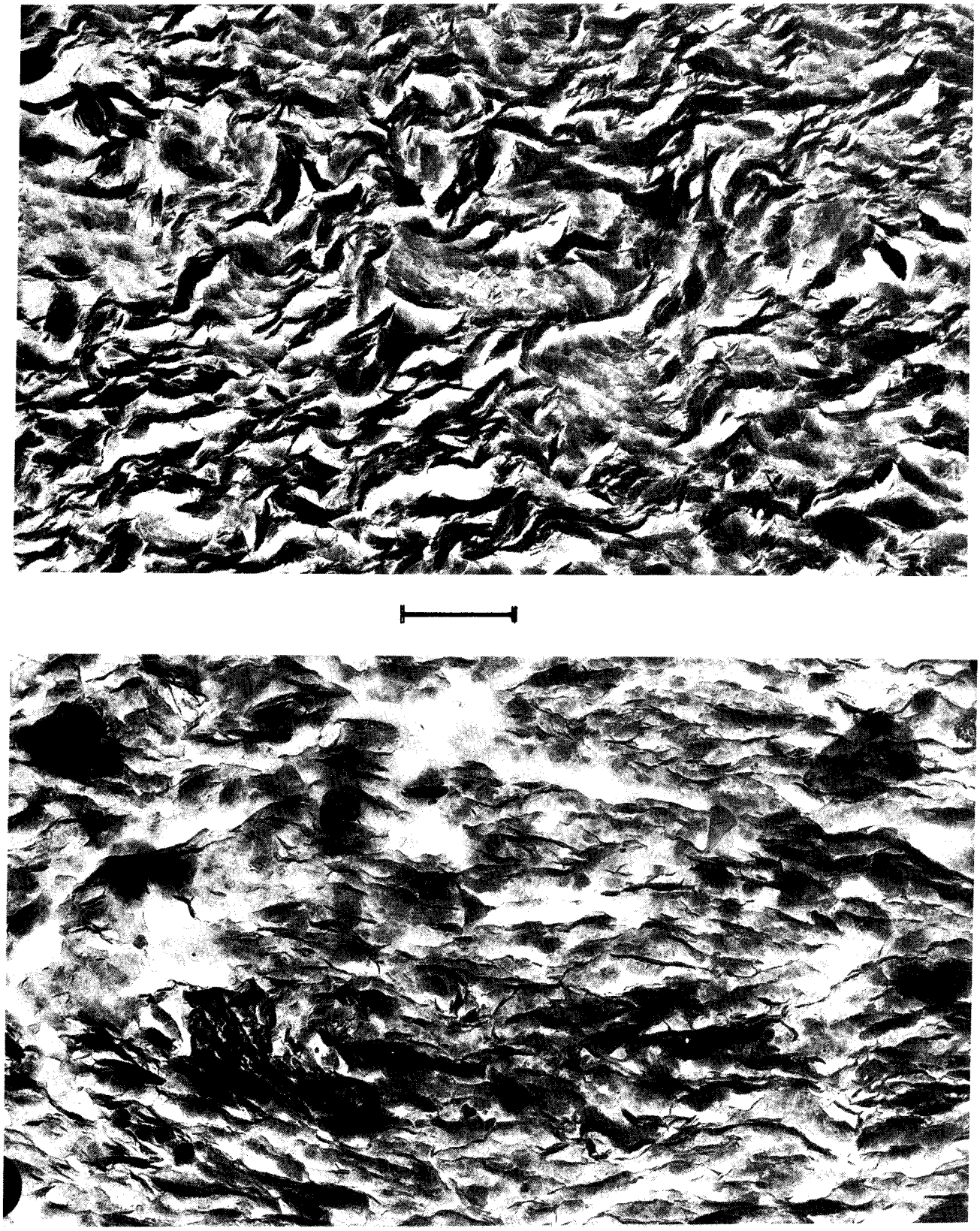

Fig. 23. Electron micrographs of Hamra clay (upper) and unheated Bavarian Ca montmorillonite, both with a bulk density of about 2.1 g/cm^3. Scale is 1 micron

Fig.24. Electron micrograph of Hamra clay showing dense I/S stacks and neoformed illite in a large pore (upper right). Scale is 0.1 micron

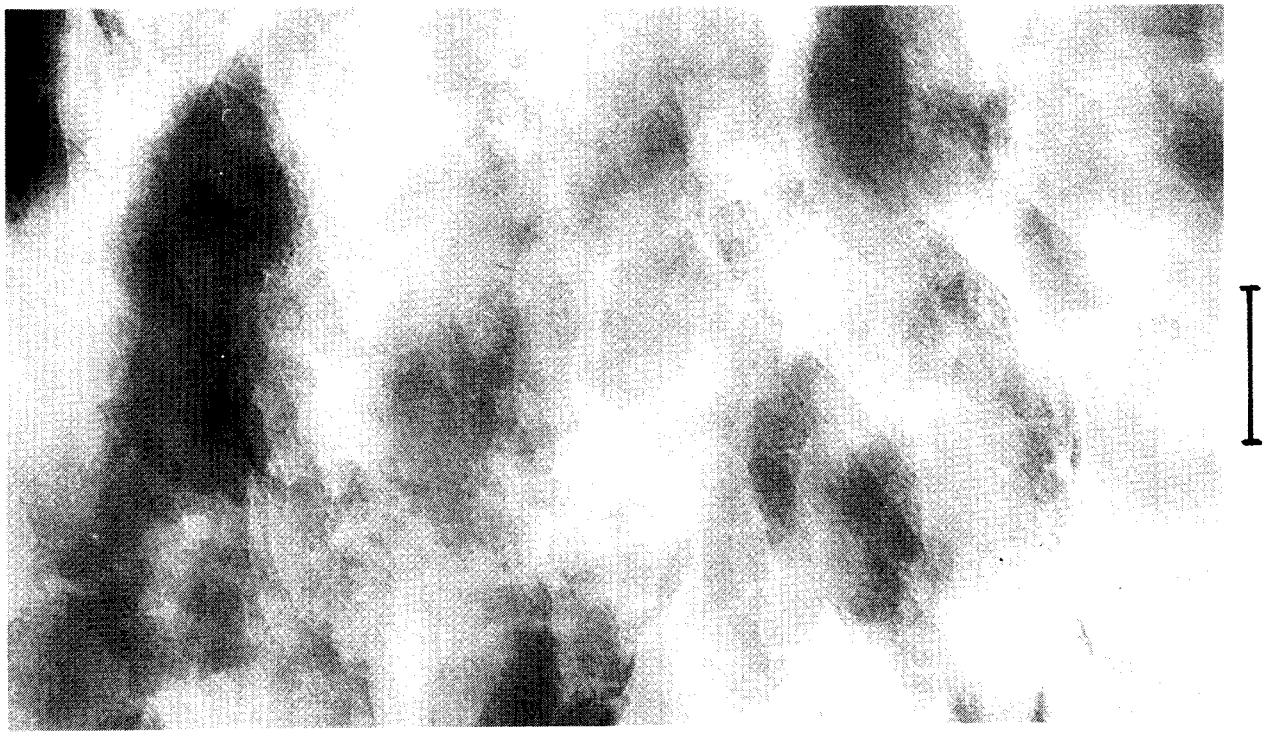

Fig.25. Homogeneous matrix of well crystallized illite in Hamra clay. Scale is 0.1 micron

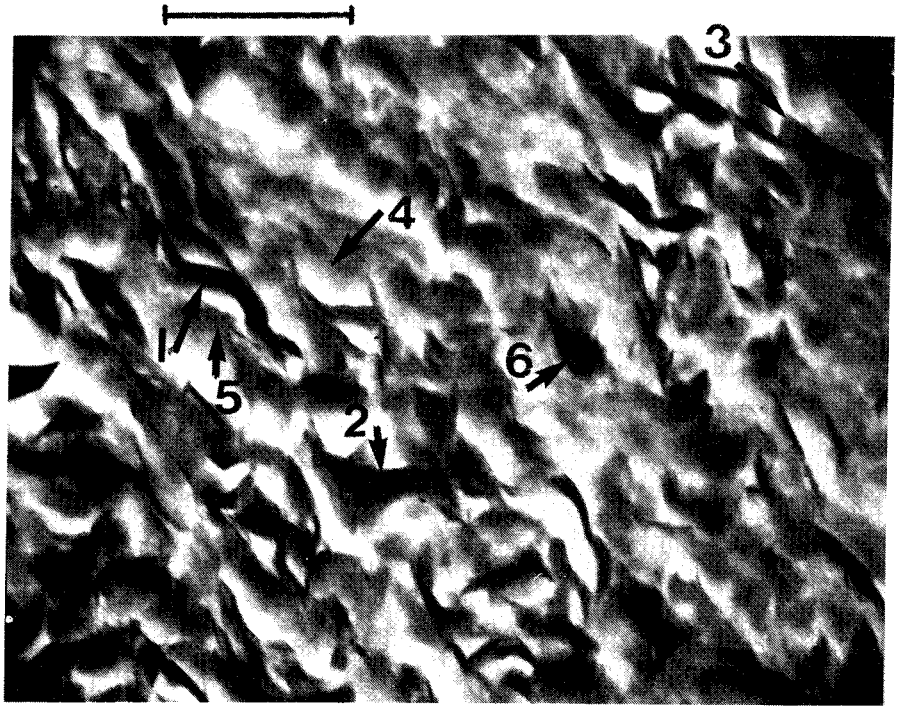

Fig.26. Microstructural region for elemental analysis. Scale is 1 micron

Spot analyses were also made for quantitative determination of Si, Al, and K, the location of the about 5000 $Å^2$ large areas being taken so that microstructurally different objects were investigated (1-6 in Fig.26). The relative concentrations are given in Table 9 and one concludes from these values that the six objects have approximately the same Si and Al compositions and that they are smectitic. Much larger variations are found in the distribution of K and it is clear that the homogeneous clay matrix (Spot 4) is particularly rich in potassium. The presence of K also in the stacks may only be apparent since neoformed illite is naturally present also in the microvoids of the stacks. It should be noted that the K concentration figures may be somewhat uncertain due to the tendency of alkali ions to migrate out of spot-analyzed areas at prolonged radiation.

It is concluded that the microstructural and elemental investigations strongly support the idea that the clay fraction consists of about 75 % mixed-layer I/S and 25 % pure illite. Furthermore, they do not contradict the hypothesis that Ca or Na are locked in the collapsed component of the I/S material. The content of smectite of the I/S material, which is probably montmorillonite in Ca form, is 40 - 50 % .

Table 9. Element concentrations in Spots 1-6 (Fig.26)

Spot	Si	Al	Mg	K	Ca	Remark
1	71	17	2	9	0.7	
2	71	17	1.6	10.5	0.0	
3	70	19	2.8	7.3	0.8	
4	69	18.7	1.7	11.3	0.0	
5	69	16	4.1	10.6	0.6	
6	69	18.9	1.5	10.1	0.4	
	66	19.4	1.2	12.1	1.1	Average

2.2.5 Geotechnical properties

2.2.5.1 *Swelling pressure, hydraulic conductivity*

The hydraulic conductivity, swelling pressure, and rheological properties were determined by testing undisturbed samples that were trimmed from the larger pieces of which the core consisted. The initially unsaturated clay was contacted with artificial Forsmark water* under confined conditions which yielded a bulk density of 2.09 g/cm^3, corresponding to a dry density of 1.73 g/cm^3 and a water content of about 22 % . At that density the clay, percolated perpendicularly to the plane of sedimentation, was 5x10^{-13}m/s. It was then compressed under the effective pressure 5 MPa, which gave the bulk density 2.15 g/cm^3, and subsequently allowed to expand to 2.13 g/cm^3, which gave a swelling pressure of about 3 MPa.

* Chlorides of sodium, magnesium, and potassium dissolved in distilled water to a total salt content of 11820 ppm, with the ionic strengths: Na^+ 2530 ppm, Ca^{2+} 950 ppm, Mg^{2+} 21.7 ppm, and K^+ 5.4 ppm

2.2.5.2 *Rheological properties*

The undisturbed sample, saturated with artificial Forsmark water to a bulk density of 2.09 g/cm^3 and tested with respect to the hydraulic conductivity and swelling behavior, was thereafter consolidated under the effective pressure 7.5 MPa in the 2 cm diameter shear box, by which the net bulk density increased to 2.16 g/cm^3. The pressure, which is approximately equal to the existing effective pressure on the clay at about 515 m depth, was maintained during the creep tests. The shear stress was increased stepwise and the strain recorded and evaluated as in the Busachi case. Fig.27 shows the relationship between time, strain, and strain rate, for two characteristic load steps. We see from the smooth behavior that the clay is not cemented.

It is an important fact that the creep behavior is very similar to that of almost equally dense MX-80 clay, as illustrated by the graph in Fig.28. Thus, the fact that the shear modulus is on the same order of magnitude for both clays would suggest that the stress transfer between the microstructural units in the two smectitic clays is of the same kind. However, at the application of the load step subsequent to the 990 kPa step in the Hamra test, i.e. the one which yielded failure, the behavior was much more ductile than that of MX-80 and this is assumed to be due to the fact that shear took place along the plane of sedimentation, to which most I/S stacks are more or less parallel. The failure shear stress was 1.32 MPa.

A second creep test, using a sample that was saturated with distilled water and exposed to a normal effective pressure of only 2.5 MPa, showed approximately the same general creep behavior but an even stronger ductility. Thus, the failure strain was more than twice that at the first-mentioned test, which indicates large microstructural slip and considerable self-healing before breakdown took place. The fact that the shear stress at failure was 0.44 MPa shows that the shear strength, expressed in terms of the angle of internal friction, was the same in both clays.

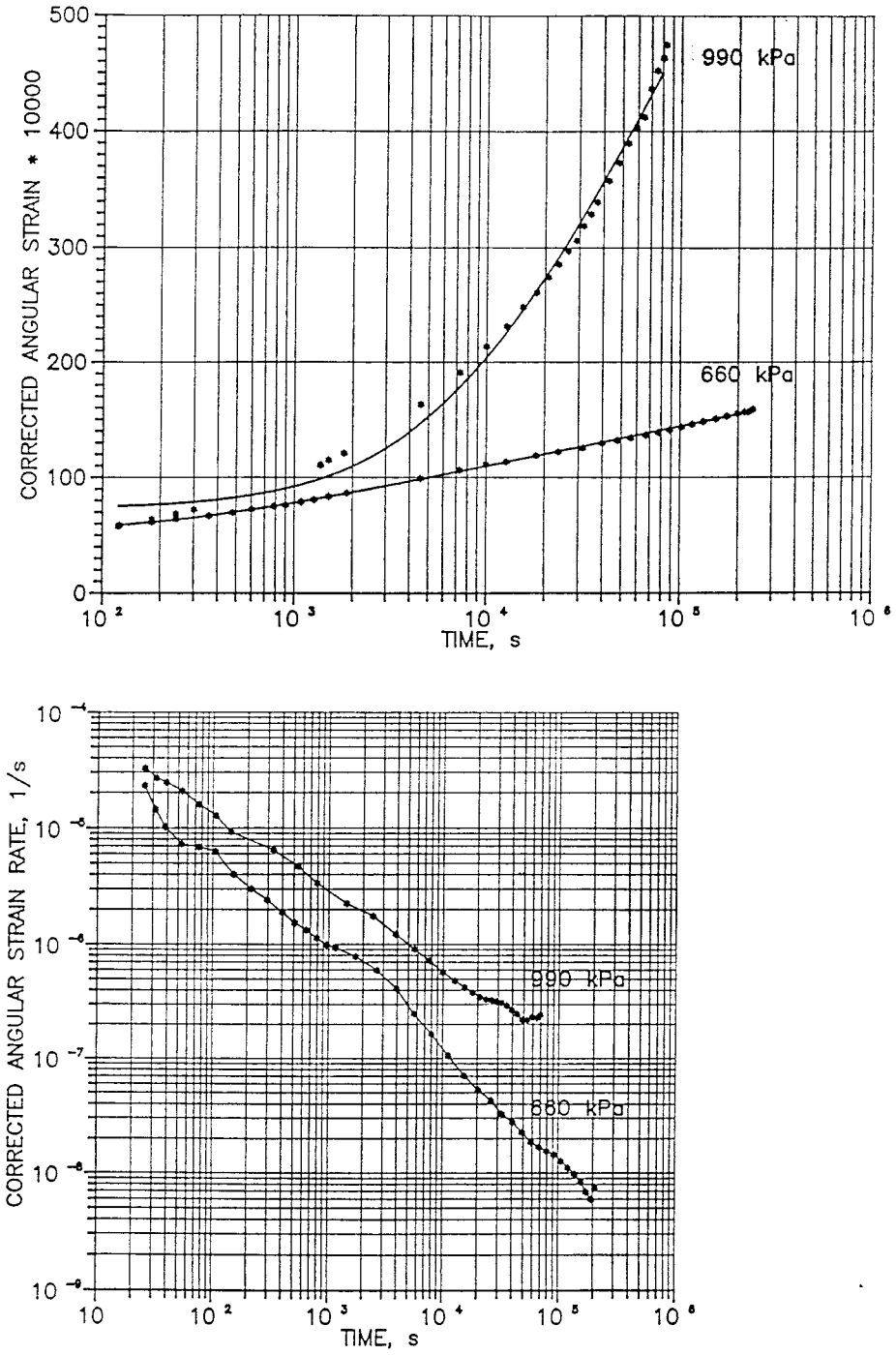

Fig.27. Creep strain versus time (upper), and strain rate versus time of the Hamra clay

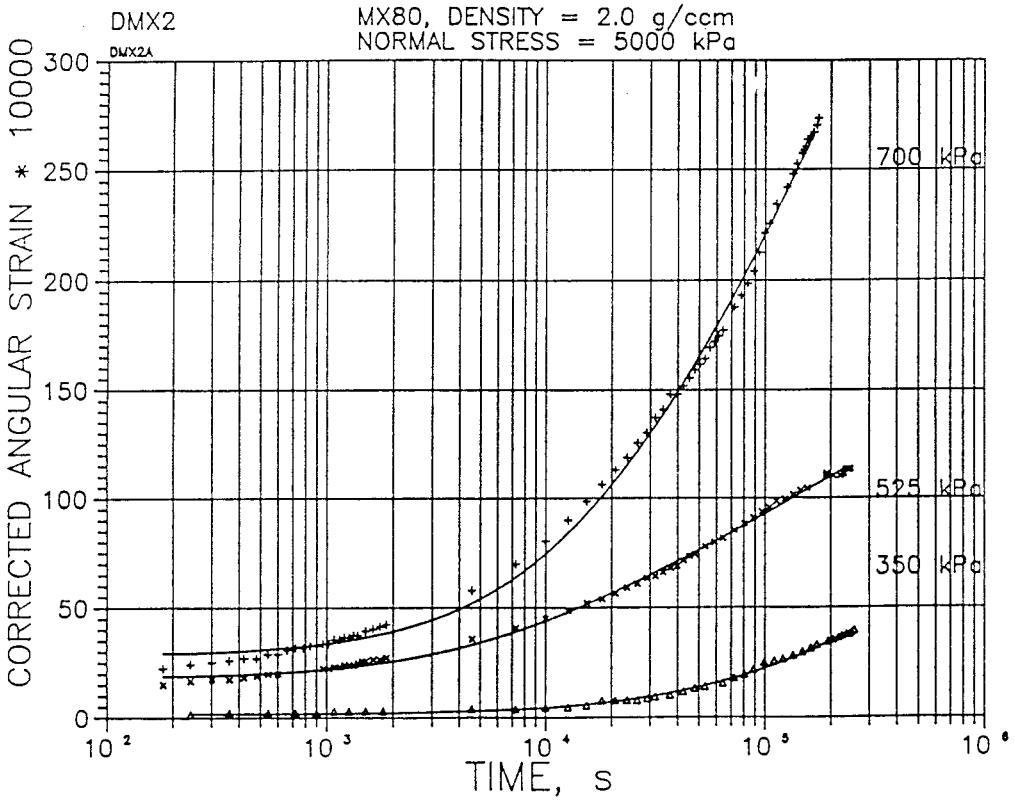

Fig.28. Creep strain versus time for MX-80 with a bulk density of 2.0 g/cm^3

2.2.6 Conclusions

The major conclusions from the investigations of the Hamra clay concern the mineralogical composition and its implications on the sealing properties. They are listed in the following way and will be commented on in this chapter and further discussed in the final chapter:

1. Assuming the initial clay sediment to have been rich in montmorillonite, it has been altered to a system of of apparent mixed-layer I/S (hydrous mica/montmorillonite) minerals and pure, neoformed illite. The I/S material may very well be hydrous mica with locked-in Na or Ca instead

of K. The clay fraction has a content of smectite (montmorillonite) of 30 - 40 %.

2. The clay is rich in potassium, which is present in fixed form in the neoformed illite but probably not in the hydrous mica component of the I/S material. The potassium source is not known and since there is no K-rich supply in the vicinity it is suspected that it may simply be the natural content of dissolved potassium in the ancient sea where sedimentation took place. The driving force in the migration process may well have been a steep concentration gradient induced by uptake and fixation of available potassium ions at the neoformation of illite. Thus, the K-accumulation as it appears today may have resulted from simple diffusion of initially present potassium in the porewater of a moderately large sediment mass.

   The Hamra clay offers an example of neoformation of illite in a smectite matrix, indicating that silica and aluminum resulted from dissolution of the smectite, and that potassium was enriched in the porewater.

3. Cementation has not taken place, which suggests that release of silica from the smectite has not been excessive. The neoformation of illite can thus be assumed to have used up silica and aluminum set free from the smectite and since this new phase only forms 25 % of the total clay fraction it is concluded that heating to 110 to 120 ^{o}C under hydrothermal conditions only causes rather insignificant dissolution of montmorillonite.

3 DISCUSSION, GENERAL CONCLUSIONS

The investigation of the Busachi and Hamra clays sheds new light on two major issues:

1) Is the mineral alteration related to time, temperature and geochemical environment? Is one of them a controlling factor?

2) Are the isolating properties of the clays sufficiently good to allow for such alteration in a repository?

We will discuss these matters in the subsequent text with special respect to the experience from hydrothermal laboratory tests and by comparing the physical data with those of earlier investigated smectitic clays.

3.1 Conditions for and processes in mineral alteration

3.2.1 General aspects

The Busachi case gives definite proof of very significant heat-induced dissolution of smectite at 150 to 200°C and precipitation of silicious material on subsequent cooling, the part of the temperature cycle that exceeded 100°C being shorter than 3 months. The precipitations are strikingly similar to those in the Ordovician Kinnekulle, which is assumed to have been heated to 110 - 160°C, and they are concluded to be responsible for the slight brittleness that is manifested by the jerky creep and reduced expandability of both clays. According to the current working model of smectite alteration (2), heating to 130 - 150°C yields complete dehydration and collapse to 10 Å spacing, which may become permanent in part of the clay mass by spot-welding of precipitated silica at the edges of the smectite stacks at the upper boundary of this temperature interval. A slight bump at d = 10 Å of the XRD diagram of the Busachi clay heated to 150 - 200°C is actually seen (Fig.5) and the fact that the shape of the diagram is akin to that of potassium-free montmorillonite clay hydrothermally treated at 200°C for 0.5 years (2) suggests that it is not a matter of illite but rather hydrous mica with calcium or possibly sodium in interlamellar positions. However, the charge change that was associated with the heat-induced release of silica gave the necessary prerequisite for illitization and the identified 10 Å component may actually be hydrous mica with

potassium in interlamellar positions. The important thing is that so little alteration to non-expandable forms took place that it supports the view that it is *the access to potassium after the charge change* that determines the extent of alteration. Continental conditions or a very low potassium content of the environment of this 10 - 25 million years old clay series may explain the stability of the smectite.

Now, considering the Hamra clay, one would assume that release of tetrahedral silica to yield a charge deficit would hardly take place at 110 - 120°C, while such heating is expected to significant congruent dissolution of silica, aluminum and magnesium. The heating conditions would have offered a possibility for the dissolved species to escape upwards by diffusion and to precipitate higher up in the sediment series. However, the neoformed pure illite, forming about 25 % of the clay fraction, must have obtained the larger part of its silica and aluminum from the smectite and these constituents are therefore assumed to have stayed in the system. It is very probable that the potassium content controlled both processes, such that the neoformation of illite used up the heat-released silica and aluminum and the potassium available in the water, while the precipitation of illite caused additional dissolution of smectite and continued illite formation when more potassium was successively brought in from the surroundings as a consequence of the induced concentration gradient. This would explain the rather high potassium concentration in the system without implying an excess content of this element in ancient sea water.

The conclusion from the NEWMOD calculations that a hydrous mica component in mixed-layer I/S with Na or Ca in interlamellar positions cannot be distinguished from one with locked-in K, may actually suggest that the altered smectite stacks consist of a few intact and expandable sets of flakes and a somewhat larger number of collapsed ones ("brammalite"). Since hydrothermal treatment at low effective pressure and temperatures around 120°C hardly causes permanent collapse, the Hamra case could mean that a high effective pressure, i.e. about 30 MPa, produces collapse already at a temperature of 110 to 120°C. Applying the conventional view it is assumed that the hydrous mica component of the mixed-layer material is illite, but this implies that tetrahedral silica

was actually released at this relatively low temperature, which is not probable. If the temperature was in fact significantly higher than 120°C the hydrous mica component of the I/S material may of course be illite.

3.2.2 Extension of current alteration model (2)

The Busachi and Hamra cases appear to offer excellent examples of the longevity of smectite clays under different conditions. The impression is that the preliminary model of hydrothermally induced changes that was outlined by the authors in an earlier report (2) is supported by the present study. A major tentative conclusion of very substantial importance for the repository design and the selection of an optimum content of burnt-out fuel in the canisters, is that there is a critical temperature for conversion of montmorillonite to beidellite and that further alteration to mixed-layer illite/smectite and separate illite depends entirely on the access to potassium into the system. A second conclusion is that, below this critical temperature, congruent dissolution of smectite yields silica and aluminum that are reprecipitated as pure illite at a rate and extension that is controlled by the access to potassium. The present study has contributed to the understanding of the mechanisms involved in transformation of smectite to non-expanding minerals and the following extended version of the current model is hereby suggested:

1. Smectites undergo congruent dissolution at a rate and to an extension that is determined by temperature and by the activation energy for breaking lattice bonds, as well as by the chemical composition of the solution. The process is an Arrhenius-type reaction and plays a particularly important role at temperatures exceeding 100 - 150°C.

2. At temperatures below 50 - 60°C, chemical as well as physical (microstructural) changes are negligible at stagnant porewater conditions (Busachi, Wyoming and Bavarian bentonites).

3. On heating from 60 to 105°C, contraction of the smectite stacks takes place successively down to 1 hydrate layer and this is associated with a widening of the "external" voids and increased congruent dissolution of the smectite minerals. The concentration of dissolved silica and aluminum is raised to an equilibrium state under chemically closed conditions, and neoformation of illite, using up the available potassium, is initiated at the upper temperature boundary. Under chemically open conditions, i.e. in nature, the creation of illite is slow but given a very long time, i.e. many hundreds of million years, the conversion from smectite to illite will be complete without passing through a mixed layer illite/smectite scenario.

4. In the temperature interval 105 - 150°C, further contraction of the stacks down to 0 hydrate layers takes place. Complete dehydration at 105 - 120°C is facilitated by a very high effective (and possibly also porewater) pressure. By this, permanent contraction yielding mixed-layer material containing 10 Å hydrous mica-type components with Na or Ca in interlamellar positions is produced. Formation of illite/smectite mixed-layer products is still negligible or non-existent (Hamra).

   Further dissolution of the smectite constituents is caused and the concentration of dissolved silica and aluminum increased. Under open conditions, more illite will be neoformed by uptake of potassium that is brought in from the surroundings due to the concentration gradient that is set up by the successive removal of potassium from the solution (Hamra, probably also Kinnekulle and Montana bentonites).

   On cooling, reprecipitation of smectite is expected to take place under closed conditions, while the open system will be composed of the neoformed illite and the smectite residue plus reprecipitated smectite after cooling.

5. In the temperature interval 150 - 200°C complete dehydration of the smectite stacks takes place and they reach an ultimate state of contraction. Further dissolution of the smectite material takes place and conditions for additional neoformation of illite are at hand, the process requiring uptake of more potassium which is brought in by the diffusion-type process referred to above (deeply located Gulf sediments)

   At least in the case of montmorillonite, the dissolution will no longer be congruent but excess silica, emanating from tetrahedral lattice positions, is produced in this temperature region. Under open system conditions, silica is free to diffuse from the heated clay into the surroundings, where it precipitates and may create chert on cooling (Kinnekulle). Under closed conditions /hydrothermal tests, cf (2)/ or in a rapid heating/cooling sequence (Busachi, Kinnekulle), silica is precipitated in amorphous or crystalline form yielding cementation.

   The silica lost from the lattice, amounting to as much as 25 % of the total tetrahedral silica content, is replaced by aluminum (beidellitization), which may originate from octahedral positions or, more probably, from the hot solution. In the latter case, neoformation of illite will naturally be restricted.

   Charge change is a prerequisite for formation of illite/smectite mixed-layer material. Thus, the affinity to potassium of the altered smectite stacks will yield competition between them and neoformed illite crystallite nuclei, which is expected to slow down the formation of a separate illite phase. Alternatively, the I/S formation is hindered or retarded by the neoformation of illite.

This extended model is supported by a number of recent literature data. Thus, the classical transformation hypothesis of smectite-to-illite conversion leading to continuous series of illite/smectite mixed-layers

with a smectite content progressively reducing from 100 to 0 % is in apparent conflict with recent studies by Nadeau, Inoue, Ahn & Peacor, and Lee et al, reported in the years 1983 to 1988 (10). They indicate lattice images of apparently interstratified I/S arrangements according to XRD, like those of the Hamra clay, while electron microscopy shows discrete illite domains and no evidence for interstratification.

3.2 Isolating properties

Considering first the actual physical and geotechnical properties of the Busachi clay series, we conclude that the samples prepared from the material heated to about 200°C have approximately the same hydraulic conductivity and swelling pressure as well as ability to swell, as the samples from the unheated part of the series. It is not surprising that the unheated material has by and large the same low conductivity as Ca smectite-rich clays from other commercial bentonite sources (11), but it is interesting to see that the cementation of the heated clay material is broken down by gentle preparation sufficiently much to yield a rather homogeneous, low-permeable microstructure. This suggests that tectonically induced shear of a clay that has undergone such a hydrothermal scenario reactivates the clay to a physical state that is not too different from that of unheated clay. Hence, it is clear that a heat pulse of the magnitude and duration that hit the Busachi clay series below about 1 m from the molten rock did not appreciably alter its isolating properties.

The Hamra bed has a clay content of 87 %, of which 75 % is mixed-layer minerals with 40 - 50 % smectite. Thus, smectite forms about 25 % of the total soil material. Since Ca is in the exchange positions its expandability is assumed to be rather insignificant and this is also demonstrated by the significant drop in swelling pressure even on slight expansion. The swelling pressure is, however, on the expected order of magnitude and so is the hydraulic conductivity if due respect is paid to the clay content and the overall granulometry (11, 12). The conductivity i.e. 5×10^{-13} m/s, is actually somewhat lower than foreseen but this is due to the orientation of the majority of the smectite stacks and to the presence of the neoformed, illite in the voids of the smectite network.

Considering also the absence of noticeable cementation and the very obvious ductility it is concluded that the Hamra clay offers an excellent example of how well the isolating properties of a smectite-rich clay are preserved provided that it is not heated to more than 110 to 120°C and that its density is high.

3.3 Remarks

The authors conclude that a working model of smectite longevity which is in reasonable qualitative agreement with a number of laboratory tests and geological data, is at hand. The key parameter appears to be that of potassium migration while this matter does not seem to have attracted much attention from geologists, as concluded from the very meager information on the potassium sources and migration rates in the alteration of natural bentonite beds. Nor has the question of different degrees of closure of the respective geochemical system been considered in the evaluation of the diagenetic reactions. Validation of the authors' extended smectite alteration model requires that these matters be investigated, a first approach being to apply simple diffusion theory for checking the validity of the assumption of accumulation of potassium from a dilute source like ordinary seawater, in conjunction with precipitation of potassic minerals. Also, calculation should be made of the rate of alteration with respect to the uptake of potassium for comparison with the Kinnekulle case.

Through these activities the model of smectite transformation can be tested with respect to quantitative and time-related changes. One can foresee a pattern of transformation of smectite to illite which does not pass through any I/S scenario but is otherwise similar to that proposed by Pytte /cf.(2)/, i.e. a rate of alteration that is primarily dependent on temperature up to about 150°C, with the actual access to potassium as a moderating factor. At higher temperatures, and considering repository conditions, the cooling phase will yield release and precipitation of excess silica causing cementation. Here, both neoformation of illite and I/S processes will take place causing the rapid conversion that is familiar from certain hydrothermal tests.

4 ACKNOWLEDGEMENTS

The authors like to express their gratitude to Eva Hanson, Dept. of Histology, University of Lund, for the ultramicrotomy and to Dr Reine Lindwall, Linköping University, for the larger part of the STEM analyses. Thanks are extended to Dr Sven Snäll, Swedish Geological Survey, for valuable discussions on smectite longevity, and to Mr Fred Linder, OPAB, and Dr Naz Ahmed Shaikh, Swedish Geological Survey, for getting access to core samples from Hamra. The authors also greatly appreciate the computer exercises, using the NEWMOD code, that were made by Harald Hökmark, Clay Technology AB.

5 REFERENCES

1. Erlström, M. & Pusch, R. Survey of Swedish Buffer Material Candidates and Methods for Characterization. SKB Technical Report 87-32, 1987

2. Pusch, R. & Karnland, O. Hydrothermal Effects on Montmorillonite - A Preliminary Study. SKB Technical Report 88-15, 1988

3. Pusch, R., Börgesson, L. & Erlström, M. Alteration of Isolating Properties of Dense Smectite Clay in Repository Environment as Examplified by Seven Pre-Quaternary Clays. SKB Technical Report 87-29, 1987

4. Pusch, R. Creep Mechanisms in Clay. Interdisciplinary Conf. on Mechanisms of Deformation and Fracture, University of Luleå, 1978

5. Agterberg, F.P. An Undulation of the Rate of Sedimentation in Southern Gotland. Geol. Mijnbow, Vol.20, 1958 (pp. 253 - 260)

6. Pusch, R. Geotechnical Aspects of the Interpretation of Distorted Strata in Silurian Deposits. Acta Universitatis Stockholmiensis. Stockholm Contributions in Geology. Vol.XXI:2, 1969

7. Eriksson, K.G. & Malmqvist, D. A Review of the Past and the Present Investigations of Heat Flow in Sweden. Terrestrial Heat Flow in Europe. Springer-Verlag Berlin/Heidelberg/New York 1979

8. Snäll, S. Lermineral som Paleotemperaturindikatorer - Ett Försök att Bestämma Paleotemperaturen i den Sedimentära Berggrunden på Gotland. Int. Rep. SGU BRAP 88020, 1988

9. Snäll, S. Silurian and Ordovician Bentonites of Gotland (Sweden). Acta Universitatis Stockholmiensis. Stockholm Contributions in Geology. Vol. XXXI:1, 1977

10. Guven, N. Longevity of Bentonite as Buffer Material in Nuclear Waste Repository. OECD/NEA Workshop on Artificial Clay Barriers for High Level Radioactive Waste Repositories, Engineering Geology, Elsevier Publ. Co (In press)

11. Börgesson, L. & Pusch, R. Rheological Properties of a Calcium Smectite, SKB Technical Report 87-31, 1987

12. Börgesson, L., Hökmark, H., & Karnland, O. Rheological Properties of Sodium Smectite Clay. SKB Technical Report (In press)

List of SKB reports

Annual Reports

1977–78
TR 121
KBS Technical Reports 1 – 120.
Summaries. Stockholm, May 1979.

1979
TR 79–28
The KBS Annual Report 1979.
KBS Technical Reports 79-01 – 79-27.
Summaries. Stockholm, March 1980.

1980
TR 80–26
The KBS Annual Report 1980.
KBS Technical Reports 80-01 – 80-25.
Summaries. Stockholm, March 1981.

1981
TR 81–17
The KBS Annual Report 1981.
KBS Technical Reports 81-01 – 81-16.
Summaries. Stockholm, April 1982.

1982
TR 82–28
The KBS Annual Report 1982.
KBS Technical Reports 82-01 – 82-27.
Summaries. Stockholm, July 1983.

1983
TR 83–77
The KBS Annual Report 1983.
KBS Technical Reports 83-01 – 83-76
Summaries. Stockholm, June 1984.

1984
TR 85–01
Annual Research and Development Report 1984
Including Summaries of Technical Reports Issued during 1984. (Technical Reports 84-01–84-19)
Stockholm June 1985.

1985
TR 85-20
Annual Research and Development Report 1985
Including Summaries of Technical Reports Issued during 1985. (Technical Reports 85-01-85-19)
Stockholm May 1986.

1986
TR 86-31
SKB Annual Report 1986
Including Summaries of Technical Reports Issued during 1986
Stockholm, May 1987

1987
TR 87-33
SKB Annual Report 1987
Including Summaries of Technical Reports Issued during 1987
Stockholm, May 1988

Technical Reports

1988

TR 88-01
Preliminary investigations of deep ground water microbiology in Swedish granitic rocks
Karsten Pedersen
University of Göteborg
December 1987

TR 88-02
Migration of the fission products strontium, technetium, iodine, cesium and the actinides neptunium, plutonium, americium in granitic rock
Thomas Ittner[1], Börje Torstenfelt[1], Bert Allard[2]
[1]Chalmers University of Technology
[2]University of Linköping
January 1988

TR 88-03
Flow and solute transport in a single fracture. A two-dimensional statistical model
Luis Moreno[1], Yvonne Tsang[2], Chin Fu Tsang[2], Ivars Neretnieks[1]
[1]Royal Institute of Technology, Stockholm, Sweden
[2]Lawrence Berkeley Laboratory, Berkeley, CA, USA
January 1988

TR 88-04
Ion binding by humic and fulvic acids: A computational procedure based on functional site heterogeneity and the physical chemistry of polyelectrolyte solutions
J A Marinsky, M M Reddy, J Ephraim, A Mathuthu
US Geological Survey, Lakewood, CA, USA
Linköping University, Linköping
State University of New York at Buffalo, Buffalo, NY, USA
April 1987

TR 88-05
Description of geophysical data on the SKB database GEOTAB
Stefan Sehlstedt
Swedish Geological Co, Luleå
February 1988

TR 88-06
Description of geological data in SKBs database GEOTAB
Tomas Stark
Swedish Geological Co, Luleå
April 1988

TR 88-07
Tectonic studies in the Lansjärv region
Herbert Henkel
Swedish Geological Survey, Uppsala
October 1987

TR 88-08
Diffusion in the matrix of granitic rock. Field test in the Stripa mine. Final report.
Lars Birgersson, Ivars Neretnieks
Royal Institute of Technology, Stockholm
April 1988

TR 88-09
The kinetics of pitting corrosion of carbon steel. Progress report to June 1987
G P Marsh, K J Taylor, Z Sooi
Materials Development Division
Harwell Laboratory
February 1988

TR 88-10
GWHRT – A flow model for coupled groundwater and heat flow
Version 1.0
Roger Thunvik[1], Carol Braester[2]
[1] Royal Institute of Technology, Stockholm
[2] Israel Institute of Technology, Haifa
April 1988

TR 88-11
Groundwater numerical modelling of the Fjällveden study site – Evaluation of parameter variations
A hydrocoin study – Level 3, case 5A
Nils-Åke Larsson[1], Anders Markström[2]
[1] Swedish Geological Company, Uppsala
[2] Kemakta Consultants Co, Stockholm
October 1987

TR 88-12
Near-distance seismological monitoring of the Lansjärv neotectonic fault region
Rutger Wahlström, Sven-Olof Linder,
Conny Holmqvist
Seismological Depertment, Uppsala University,
Uppsala
May 1988

TR 88-13
Validation of the rock mechanics HNFEMP code against Colorado school of mines block test data
Ove Stephansson, Tomas Savilahti
University of Luleå, Luleå
May 1988

TR 88-14
Validation of MUDEC against Colorado school of mines block test data
Nick Barton, Panayiotis Chryssanthakis,
Karstein Monsen
Norges Geotekniske Institutt, Oslo, Norge
April 1988

TR 88-15
Hydrothermal effects on montmorillonite. A preliminary study
Roland Pusch
Ola Karnland
June 1988

TR 88-16
Swedish Hard Rock Laboratory
First evaluation of preinvestigations 1986-87 and target area characterization
Gunnar Gustafson
Roy Stanfors
Peter Wikberg
June 1988

TR 88-17
On the corrosion of copper in pure water
T E Eriksen[1], P Ndalamba[1], I Grenthe[2]
[1]The Royal Institute of Technology, Stockholm
Department of nuclear chemistry
[2]The Royal Institute of Technology, Stockholm
Department of inorganic chemistry
March 1988

TR 88-18
Geochemical modelling of the evolution of a granite-concrete-water system around a repository for spent nuclear fuel
Bertrand Fritz, Benoit Madé, Yves Tardy
Université Louis Pasteur de Strasbourg
April 1988

TR 88-19
A Bayesian nonparametric estimation of distributions and quantiles
Kurt Pörn
Studsvik AB
November 1988

TR 88-20
Creep properties of welded joints in OFHC copper for nuclear waste containment
Bo Ivarsson, Jan-Olof Österberg
Swedish Institute for Metals Research
August 1988

TR 88-21
Modelling uranium solubilities in aqueous solutions: Validation of a thermodynamic data base for the EQ3/6 geochemical codes
I Puigdomenech[1], J Bruno[2]
[1]Studsvik Nuclear, Nyköping
Environmental Services
[2]Royal Institute of Technology, Stockholm
Department of Inorganic Chemistry
October 1988

TR 88-22
Radiolysis of ground water: influence of carbonate and chloride on the hydrogen peroxide production
T E Eriksen[1], P Ndalamba[2], H Christensen[2],
E Bjergbakke[3]
[1]The Royal Institute of Technology, Department of Nuclear Chemistry, S-100 44 Stockholm, Sweden
[2]Studsvik Energiteknik AB, S-611 82 Nyköping, Sweden
[3]Risö National Laboratory, DK-4000 Roskilde, Denmark
December 1988

TR 88-23
Source parameters of major earthquakes near Kiruna, northern Sweden, deduced from synthetic seismogram computation
W T Kim, E Skordas, Y P Zohu, O Kulhanek
Seismological Department, Uppsala University,
Box 12019, S-750 12 UPPSALA
June 1988

TR 88-24
Fission product concentration profiles (Sr, Xe, Cs and Nd) at the individual grain level in power-ramped LWR fuel
R S Forsyth, O Mattsson, D Schrire
Studsvik Nuclear, Nyköping
December 1988

TR 88-25
Postglacial faulting and paleoseismicity in the Lansjärv area, northern Sweden
Robert Lagerbäck
October 1988